



Applied Computational
Electromagnetics Society



Newsletter
Volume 18 - No. 2
ISSN 1056-9170



July 2003



**APPLIED COMPUTATIONAL ELECTROMAGNETICS SOCIETY
(ACES)**

NEWSLETTER

Vol. 18 No. 2

July 2003

TABLE OF CONTENTS

IN MEMORIAM: Patricia B. Adler Perry Wheless	5
COMMITTEE REPORTS Election/Nomination Committee – Rene Alard Candidate Statements	6
DEPARTMENTS Modeler’s Notes Change in NEC 4.1 Distribution Procedure – Jerry Burke	12
Practical CEMist Modular Development of CAE Models for Lossy Matching Networks: Part 1 Shaohua Li, Perry Wheless	14
TECHNICAL FEATURE ARTICLE – “CEM Code Validation Using Infrared Thermograms” John Norgard.....	20
TUTORIAL ARTICLE – “Review of Advanced Electromagnetic Modeling Techniques in the Computer Code FEKO based on the Method of Moments with Hybrid Extensions” Ulrich Jakobus	30
Analysis of the Transition Between Two Coplanar Waveguide Transmission Lines A.A. Eldek, A. Z. Elsherbeni, C.E. Smith	44
ANNOUNCEMENTS: The 21st Annual Review of Progress in Applied Computational Electromagnetics Call for Papers.....	48
APPLICATION for ACES Membership, Newsletter and Journal Subscription.....	50
ADVERTISING Rates	51
DEADLINE for Submission of Articles.....	51

ACES NEWSLETTER STAFF

EDITOR-IN-CHIEF, NEWSLETTER

Bruce Archambeault
IBM
3039 Cornwallis Road, PO Box 12195
Dept. 18DA B306
Research Triangle Park, NC 27709
Phone: 919-486-0120
email: barch@us.ibm.com

EDITOR-IN-CHIEF, PUBLICATIONS

Andrew Peterson
Georgia Institute of Technology, ECE
777 Atlantic Drive
Atlanta, GA 30332-0250
Phone: 404-894-4697
Fax: 404-894-5935
email: peterson@ee.gatech.edu

ASSOCIATE EDITOR-IN-CHIEF

Ray Perez
Martin Marietta Astronautics
MS 58700, PO Box 179
Denver, CO 80201
Phone: 303-977-5845
Fax: 303-971-4306
email: ray.j.perez@lmco.com

MANAGING EDITOR

Richard W. Adler
Naval Postgraduate School/ECE Dept.
Code ECAB, 833 Dyer Road, Room 437
Monterey, CA 93943-5121
Phone: 831-646-1111
Fax: 831-649-0300
email: rwa@attglobal.net

EDITORS

CEM NEWS FROM EUROPE

Pat R. Foster
Microwaves and Antenna Systems
16 Peachfield Road
Great Malvern, Worc. UK WR14 4AP
Phone: +44 1684 5744057
Fax: +44 1684 573509
email: prf@maasdesign.co.uk

TECHNICAL FEATURE ARTICLE

Andy Drozd
ANDRO Consulting Services
PO Box 543
Rome, NY 13442-0543
Phone: 315-337-4396
Fax: 314-337-4396
email: androl@aol.com

THE PRACTICAL CEMIST

W. Perry Wheless, Jr.
University of Alabama
PO Box 11134
Tuscaloosa, AL 35486-3008
Phone: 205-348-1757
Fax: 205-348-6959
Email: wwheless@ualvm.ua.edu

MODELER'S NOTES

Gerald Burke
Lawrence Livermore National Labs.
Box 5504/L-156
Livermore, CA 94550
Phone: 510-422-8414
Fax: 510-422-3013
email: burke2@llnl.gov

PERSPECTIVES IN CEM

Manos M. Tentzeris
Georgia Institute of Technology
ECE Dept.
Atlanta, GA 30332-0250
Phone: 404-385-0378
email: eentze@ece.gatech.edu

TUTORIAL

J. Alan Roden
IBM Microelectronics
Dept. OSXA
3039 Cornwallis Road
Research Triangle Park, NC 27709
Phone: 919-543-8645
email: jaroden@us.ibm.com

ACES JOURNAL

EDITOR IN CHIEF

Atef Elsherbeni
EE Department, Anderson Hall
University of Mississippi
University, MS 38677
Phone: 662-915-5382
email: atef@olemiss.edu

NEWSLETTER ARTICLES AND VOLUNTEERS WELCOME

The ACES Newsletter is always looking for articles, letters and short communications of interest to ACES members. All individuals are encouraged to write, suggest or solicit articles either on a one-time or continuing basis. Please contact a Newsletter Editor.

AUTHORSHIP AND BERNE COPYRIGHT CONVENTION

The opinions, statements and facts contained in this Newsletter are solely the opinions of the authors and/or sources identified with each article. Articles with no author can be attributed to the editors or to the committee head in the case of committee reports. The United States recently became part of the Berne Copyright Convention. Under the Berne Convention, the copyright for an article in this newsletter is legally held by the author(s) of the article since no explicit copyright notice appears in the newsletter.

BOARD OF DIRECTORS

EXECUTIVE COMMITTEE

Osama Mohammed, President	Allen W. Glisson, Treasurer
Bruce Archambeault, Vice President	Richard W. Adler, Executive Officer
Keith Lysiak, Secretary	

DIRECTORS-AT-LARGE

Masanori Koshiba	2003	Bruce Archambeault	2004	Allen W. Glisson	2005
Osama Mohammed	2003	Andrzej Krawczyk	2004	Keith Lysiak	2005
Tapan Sarkar	2003	Ray Perez	2004	Eric Mechielssen	2005

ACES ELECTRONIC PUBLISHING GROUP

Atef Eisherbeni	Electronic Publication Managing Editor
Matthew J. Inman	Site Administrator
Jessica Drewrey	Assistant Administrator
Brad Baker	Contributing Staff
Imran Daker	Past Administrator
Chris Riley	Past Staff

Visit us on line at:
<http://aces.ee.olemiss.edu>

PERMANENT STANDING COMMITTEES OF ACES, INC.

COMMITTEE	CHAIRMAN	ADDRESS
NOMINATIONS	Rene Allard	Penn State University PO Box 30 State College, PA 16804-0030
ELECTIONS	Rene Allard	Penn State University PO Box 30 State College, PA 16804-0030
FINANCE	Allen Glisson	EE Department Anderson Hall University of Mississippi University, MS 38677
PUBLICATIONS	Andrew Peterson	Georgia Institute of Technology School of ECE Atlanta, GA 30332-0250
CONFERENCE	Osama Mohammed	Florida International University ECE Department Miami, FL 33174
AWARDS	Pat Foster	MAAS 16 Peachfield Road Great Malvern, UK WR14 4AP

MEMBERSHIP ACTIVITY COMMITTEES OF ACES, INC.

COMMITTEE	CHAIRMAN	ADDRESS
SOFTWARE VALIDATION	Bruce Archambeault	IBM 158 Lin Tilley Road Durham, NC 27712
HISTORICAL	Robert Bevensee	BOMA Enterprises PO Box 812 Alamo, CA 94507-0812

In Memoriam: Patricia B. Adler

It is with great sadness that we announce the passing on March 25, 2003, of Pat Adler, administrative assistant for the Applied Computational Electromagnetics Society since its inception in 1985. Over its eighteen years of operation, she gave an extraordinary amount of time and effort, at the highest professional level, to promoting and advancing ACES.

Introduced to the community of applied computational electromagnetics practitioners through her husband, Pat embraced his worldwide colleagues as members of her extended family. Her kind consideration and cheerful demeanor won her many close friends in ACES. Beyond her careful attention to the business of the society and respect for each member she dealt with, those of us who came to know her personally appreciated her sincere concern for our personal welfare. Pat extended warm friendship and innumerable small kindnesses to thousands of Annual Review of Progress conference attendees, especially international visitors, and her smiling greeting at the registration desk was a pleasant annual anticipation. She was a superb advocate for ACES, and her role in local arrangements was key in securing the annual conference as the centerpiece activity of ACES.

Born a Pennsylvanian, Pat Adler found her destined home in Monterey after Dick received the Ph.D. degree from Penn State in 1970 and joined the Naval Postgraduate School faculty. Pat also worked as a Naval Postgraduate School staff member early on, but later devoted her fulltime attention to the combined duties of administrative assistant for ACES and homemaker for a growing family of children and grandchildren. She loved and thoroughly enjoyed both the environment and vibrant spirit of the Monterey Peninsula.

Pat was a person of deep religious conviction. The strong and abiding faith she found through The Church of Jesus Christ of Latter-Day Saints guided and illuminated her life. Mormons are widely known and respected for living daily lives that honor and reflect their spiritual principles, and for their strong desire to be a positive influence on everyone they meet. Pat was a worthy emissary and, indeed, a positive influence on all those who came to know her. Among the beneficiaries of her faith are some thirty-nine children who, in their time of crisis and greatest need, found a foster home with the Adler family.

ACES was founded largely to provide an alternative to existing organizations dominated by a majority view and agenda that actively discouraged the healthy exchange of new and "different" developments in the emerging science of computational electromagnetics. In particular, ACES has been uniquely receptive to reports dealing with practical applications. Pat was rightfully proud of her contributions to providing an influential outlet, through ACES publications and the annual conference, for the public distribution and archival preservation of many meritorious works. The fruits of her labor on behalf of ACES, for which we are all deeply grateful, will continue to grow in the future, and are part of her legacy.

We trust that, for Pat, joy and rejoicing have now banished all pain, griefs, and anxious fears. With faith in the hope of the resurrection, we long to see her again when our days on Earth are done.

Perry Wheless

CANDIDATES STATEMENTS
2003 ELECTION FOR THE BOARD OF DIRECTORS

DR. ALKIM AKYURTLU



GENERAL BACKGROUND

Alkim Akyurtlu was born in Madison, WI, in November 1972. She earned her B.S.E.E. at Virginia Polytechnic Institute and State University (Virginia Tech) in 1994. She earned the M.S. and Ph.D. degrees in Electrical Engineering at the Pennsylvania State University in 1996 and 2001, respectively. During her graduate studies, she was an Academic Computing Fellow, she won the ACES Best Student Paper Contest in 2000, and the Anthony Ferraro Best Doctoral Research Award in 2001.

After graduation Dr. Akyurtlu joined the Systems and Analysis Group at MIT Lincoln Laboratory, where she worked on statistical analysis of radar systems and applications of meta-materials.

Currently, she is an Assistant Professor in the Electrical and Computer Engineering Department at University of Massachusetts Lowell where she is conducting research in computational electromagnetics, teaching courses on antenna theory and radar systems, and supervising the research of M.S. and Ph.D. students. Prof. Akyurtlu's current research interests include computational electromagnetics with applications in meta-materials and antennas, and micro- and nano-scale device modeling. Prof. Akyurtlu has been awarded the NASA Faculty Fellowship Award for 2003 and the Teaching Award in the Electrical Engineering Department at UMass Lowell for the 2002-2003 academic year.

Dr. Akyurtlu is a member of ACES and the IEEE Antennas and Propagation and Microwave Theory and Techniques Societies.

PAST SERVICE TO ACES

The candidate's past service to ACES includes presentation of papers at the 2000 and 2001 ACES Conferences.

CANDIDATE'S PLATFORM

Computational electromagnetics has been very successful in answering the many complicated questions in the field of electromagnetics. It will play an even more important role in the future as we move into new ways of thinking about conventional problems at the nano-scale levels. Integration of electromagnetics with other research areas will also be very significant in the development of new technologies. I believe that ACES will be an integral venue to carry the area of computational electromagnetics into exciting future frontiers, increase interdisciplinary research, and raise the focus on applications of computational electromagnetics in the advanced technologies. In order to accomplish the aforementioned goals, advertisement of ACES activities and seminars so as to attract the most recent advances in the area of computational electromagnetics and relevant interdisciplinary research is necessary. I would like to contribute

to increasing participation in ACES and to continuing to make this society an arena for advancing technology. ACES is very important in bringing the electromagnetics community together and in exposing the newest and most significant advancements in the application of computational electromagnetics and should continue to maintain its strong role in the future.

DR. RANDY HAUPT



GENERAL BACKGROUND

Randy Haupt is an IEEE Fellow and Professor and Department Head of Electrical and Computer Engineering at Utah State University. He has a Ph.D. in Electrical Engineering from the University of Michigan, MS in Electrical Engineering from Northeastern University, MS in Engineering Management from Western New England College, and BS in Electrical Engineering from the USAF Academy. He was a Professor of Electrical Engineering at the USAF Academy and Professor and Chair of Electrical Engineering at the University of Nevada Reno. Randy was a project engineer for the OTH-B radar and a research antenna engineer for Rome Air Development Center. His research interests include genetic algorithms, antennas, radar, numerical methods, signal processing, fractals, and chaos. He was the Federal Engineer of the Year in 1993 and is a member of Tau Beta Pi, Eta Kappa Nu, URSI Commission B, and Electromagnetics Academy. He has numerous journal articles, conference publications, and book chapters on antennas, radar cross section and numerical methods and is co-author of the book *Practical Genetic Algorithms*, John Wiley & Sons, Jan 1998. Randy has eight patents in antenna technology and is director of the Utah State University Anderson Wireless Center. He teaches courses in antennas and computational electromagnetics.

PAST SERVICE TO ACES

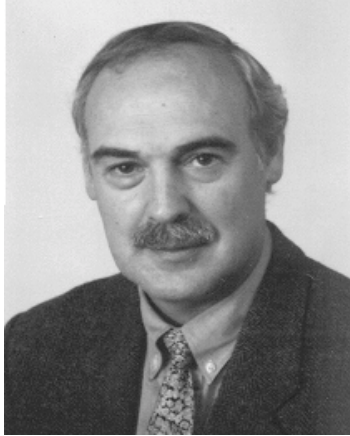
- Received ACES Valued Service Award in 2000
- Guest Editor for ACES Journal special issue on genetic algorithms in Jul 00
- Conference Chair for 1999 ACES International Symposium
- Co-chair of ACES conference Mar 1998
- Co-chair of ACES conference Mar 2000
- Presented ACES short courses in 97, 98, 99
- Took 8 ACES short courses
- Served as session chair at ACES conferences
- Presented 11 papers at ACES Conference
- Attended 10 ACES conferences

CANDIDATE'S PLATFORM

- I have always liked ACES because of its practical focus. I would continue to emphasize and expand this focus. The publications, the conference, the web site, and the short courses should be excellent references for members. Perceived value will result in growth.

- The international participation in ACES is extremely valuable and every effort should be made to encourage a broad participation.
- Some effort should be made to improve the impact factor of the ACES Journal.
- It would be worthwhile to have book reviews and software reviews for members.
- I would like to encourage the presentation of new and interdisciplinary approaches to computational methods.

DR. JUAN R. MOSIG



GENERAL BACKGROUND

Juan R. Mosig was born in Cadiz, Spain. He received his Telecommunication Engineering Degree (M. Sc. E.) from the Polytechnic University of Madrid, Spain in 1974 and the Ph.D. degree from the Swiss Institute of Technology (Ecole Polytechnique Fédérale) of Lausanne, Switzerland in 1983.

In 1985 he was a Senior Research Associate at R.I.T., Rochester, NY, working for DEC in a project under the direction of Prof. T. K. Sarkar. He has also held summer scientific appointments at University of Colorado at Boulder, CO, Technical University of Denmark, Universities of Rennes and Nice in France and University of Rome-La Sapienza in Italy.

Since 1991 he has been a professor at EPFL and since 2000 the Head of the EPFL Laboratory of Electromagnetics and Acoustics (LEMA). In 2003 he became the Director of the Institute for Transmissions, Electromagnetic Waves and Photonics (iTOP).

Dr. Mosig is the author of four chapters in books on microstrip antennas and circuits and more than hundred reviewed papers. He received twice the Best Paper Award at the JINA Conference on Antennas (Nice, France) and he is now a member of its Steering Committee. His research interests include electromagnetic theory, numerical methods and planar antennas and he is a Fellow of the IEEE.

Since 1987, Dr. Mosig has been actively involved in the organization of intensive short courses in Numerical Electromagnetics in the USA (with University of Syracuse NY, Boulder Microwave Technology, Ansoft...) that he has successfully introduced in Europe. He has been a member of the IEEE Antennas and Propagation Society AdCom as responsible of Transnational Activities. In 2000, Dr. Mosig was the Head of the National Swiss Committee for the European Millennium Antenna and Propagation Conference, organized by the European Space Agency in Davos, Switzerland.

Dr. Mosig has been a Steering Committee Member in the European Research programme MADS (Multipurpose Antenna Design Simulator, 1998-2002) which put together leading European universities and industrial R&D groups, targeting for the first time the development of a "universal antenna numerical tool". This effort is currently being pursued under a grant from the European Space Agency. He is also the Swiss representative in the European project "FractalComs" aiming at the electromagnetic analysis of fractal geometry antennas and a member of the European "Research Training Network MMCODEF", whose goal is the exchange of postgraduate students between participant European universities and subsequent training in the European microwave industries.

Since 1999, Dr. Mosig is a member, nominated by the Swiss Federal Government, of the Technological Policy Advisory Committee for the Swiss Space Office. He is also technical advisor for the curricula program of several newly created Polytechnic Universities in Spain.

Dr. Mosig is the responsible for introducing by the first time (year 2000) a session in Computational Electromagnetics in the European Congress on Computational Methods in Applied Science and Engineering (ECCOMAS), where is a member of the Technical Committee.

Currently, Dr. Mosig is the Chairman of an European COST (Scientific and Technological European Cooperation) Action, the COST-284 project "Innovative Antennas for Emerging Terrestrial and Space-based applications", which is a five years (2002-2006) project with the participation of 19 European countries aiming at fostering the development of antenna and electromagnetic research in Europe and including an active Working Group on antenna design softwares.

PAST SERVICES TO ACES

The candidate has contributed with several papers to ACES Symposia, which he considers the most adequate venue for presentation and dissemination of research works in numerical electromagnetics

CANDIDATE'S PLATFORM

With the increasing widening of electrical engineering domains and the consequent lack of focus of its traditional societies, ACES should now be the obvious society for any researcher, scientist or engineer concerned with Numerical Electromagnetics. I would like to strongly support this idea not only in the USA but elsewhere in the world and especially in Europe. ACES publications and ACES Symposia should become the reference for theoreticians, code developers and code users in the area of Electromagnetics.

At the research level, I believe that we need to strength the link from fundamental theoretical research and numerical applications, since tomorrow's successful commercial codes will be based in today's advanced mathematical algorithms. Also, Applied Computational Electromagnetics should explore more deeply the possible parallels and synergies with other engineering domains where numerical and computational methods play an important role. I think that we can still borrow many useful ideas from Fluid and Structural Mechanics or from Civil and Chemical Engineering, and in turn show to them the richness of Computational Electromagnetics and the specificity of our implementations. In this respect, the introduction of a "Computational Electromagnetic area" in the ECCOMAS Symposium has been a very positive experience and I would like to explore further possibilities of these synergies.

I am fully committed to engineering education and I believe ACES can play an essential role in influencing the future curricula for Bachelor, Master and Ph.D. programmes, not only in the USA but elsewhere in the world. In Europe, we are striving for keeping alive the teaching of courses in Numerical Electromagnetics at both undergraduate and postgraduate levels and ACES should provide an excellent source and frame for an active campaign in this direction. In parallel, ACES Conferences should be better advertised and their associated short courses systematically connected with University credits in order to encourage participation of young researchers which would look afterwards at ACES as a top professional society.

OTHER UNIQUE QUALIFICATIONS

Being actively present in both Higher Education (as an University Professor in a leading European Institute of Technology) and in Applied Electromagnetics Research (as a leader of a team deeply involved in many high-end numerical electromagnetics projects at the European level), I think I have an excellent vantage position to work towards the consecution of above mentioned goals. Moreover, in my role of Chairman of an European COST Action, I have excellent links with all the European Research Institutes in our domain and also in parallel engineering areas, where equivalent computational tools are used. I am currently involved in an ambitious proposal for creating a European Union "Network of Excellence on Antenna Research". If successful, this Network could become a privileged partner of ACES and contribute to the ACES worldwide recognition.

DR. OMAR RAMAHI



GENERAL BACKGROUND

Omar M. Ramahi received the BS degrees in Mathematics and Electrical and Computer Engineering, with highest honors, from Oregon State University, Corvallis, OR in 1984. He received his M.S. and Ph.D. in Electrical and Computer Engineering in 1986 and 1990 respectively from the University of Illinois at Urbana-Champaign. From 1990-1993, he held a visiting fellowship position at the University of Illinois at Urbana-Champaign including a one-year appointment as a Postdoctoral Fellow working with the Professor Y. T. Lo on microstrip antenna problems. In 1993, he joined Digital Equipment Corporation as a member of the Technology Development Group. In 1994 he became a member of the alpha server product development group at the same company. In August of 2000, he joined the faculty of the A. James Clark School of Engineering at the University of Maryland at College Park, where he presently holds a faculty appointment in the Mechanical Engineering Department and an affiliate appointment in the Electrical and Computer Engineering Department. Professor Ramahi is also a faculty member of CALCE Electronics Products and Systems Center at the University of Maryland.

Dr. Ramahi served as a consultant to several companies. He was instrumental in developing computational techniques to solve a wide range of electromagnetic radiation problems in the fields of antennas, high-speed devices and circuits and EMI/EMC. He has developed computational electromagnetic codes based on the Method of Moments, the Finite Element method, the Finite-Difference Time-Domain method, amongst others. His interests include theoretical, experimental and computational EMI/EMC studies, high-speed devices and interconnects, biomedical applications of electromagnetics, novel optimization techniques, interdisciplinary studies linking electromagnetic application with new materials. He has authored and co-authored over 110 journal and conference papers and presentations. He is a co-author of the book *EMI/EMC Computational Modeling Handbook*, 2nd Ed., (Kluwer Academic, 2001). Dr. Ramahi is a member of Eta Kappa Nu and Tau Beta Pi honor societies. He is also a Senior Member of IEEE and a member of the Electromagnetics Academy.

PAST SERVICE TO ACES

The candidate's past service to ACES includes presentation of numerous papers, organization of special sessions for the ACES Symposia and participation as short course instructor.

CANDIDATE'S PLATFORM

The field of electromagnetism (EM) is probably one of the very few fields in applied science that has reached a high level of maturity. Computational electromagnetism, which is considered the applied side of electromagnetism, has witnessed an explosive growth in the past fifteen years. Today, we have numerical algorithms that can characterize wave-matter electromagnetic interaction with a high degree of accuracy and with sufficient speed. Despite the maturity in both theoretical and computational electromagnetism, the application of computational EM to new technological frontiers remains in its infancy. For instance, in the emerging field of nanotechnology, sensors, biomedical devices, amongst others, electromagnetism is expected to play a significant role. For computational EM practitioners, the primary challenge is in the fact that these new technologies are driven by strong interdisciplinary research teams that are typically devoid of computational EM experts. Interestingly enough, the classical EM practitioner paradigm has changed. Instead of using computational EM to solve known problems, we need to look at applications that can be designed by harvesting the power of EM with the aid of computational EM.

Having the vintage point of working with mechanical, electrical, and aerospace engineers in the emerging technologies, I have the advantage of identifying new and significant applications of computational EM and bring these applications to the EM community through ACES. Furthermore, bringing a strong focus to ACES activities and seminars would be a priority. Despite the plethora of symposia and technical societies involved in electromagnetics, there is a distinct place for a society, such as ACES, which is devoted exclusively to practical computational electromagnetics. For this reason, ACES needs to have a strong focus through symposia and published media that reinforces its distinct thrust. The ACES annual meeting has been suffering in the past few years from lower attendance than in the earlier years. This phenomenon needs to be addressed and structural changes might become necessary to maintain the vitality, strength and relevance of ACES. These are some of the issues that I like to address if I become a Board Member.

Change in the NEC-4.1 Distribution Procedure *

Gerald J. Burke
Lawrence Livermore National Laboratory
P.O. Box 808, L-154, Livermore, CA 94550
burke2@llnl.gov

After years of saying that the distribution procedure and restrictions on NEC-4.1 were about to change it has finally happened. The licensing of NEC-4 is now handled by the Industrial Partnerships and Commercialization (IPAC) office at LLNL. Information on the licensing procedure and a license form can be found at the website

<http://www.llnl.gov/software/software.php>

The program remains under copyright to the University of California that restricts release and distribution. However, after reviewing the code they have determined that export control is not needed except for countries on the DoE “sensitive country” list. Saddam need not apply. IPAC has increased the licensing fee to \$950, but has set a \$250 fee for academic and “non-commercial” use. The qualifications for “non-commercial” will be determined by IPAC, but it should ease the bite for people such as Amateur Radio operators.

When we were handling the distribution we could send out the code when we had received the registration form and a check or purchase order. IPAC does not accept purchase orders, but needs the license form and a check. They said that they may be able to accept credit card orders, but I don’t think that has been tried yet. When they have everything that they need, they let me know that it OK to send the code.

There is not much information on the IPAC website on what is included in the NEC-4.1 package, but it is the same as before. We send out a CD with the source codes in single and double precision and the plotting programs for Windows. Executable files are included compiled for various matrix sizes, typically 1200, 2000, 3600 and 7500 segments for in-core matrix storage. A printed copy of the manuals is include as well as a scanned (bit-mapped) copy on the CD. Source files with Windows specific calls removed are included for unix systems.

In many ways NEC-4 is the same as NEC-2. The basic code reads an input file that describes the model and requests calculations of currents and fields. The code package includes programs to plot and check the model geometry and to plot impedance versus frequency on Cartesian or Smith charts with an option for rational-function interpolation over frequency, sometimes called “fast frequency sweep”. There is also a program to plot radiation patterns in Cartesian or polar plots or as 3D patterns with hidden lines removed.

The major features that NEC-4 offers over NEC-2 are the ability to model wires in the ground, such as buried antennas, ground stakes and ground screens, and a model for wires with a thin insulating sheath. With NEC-2 you had to run a separate program to generate the Sommerfeld integral tables for ground. NEC-4 will look for a file and generate it if a matching file for the model is not found. When a frequency loop is run it will generate a family of files with incremented names. Then when a new run is made it will reuse the files if they match.

At least as important as these features is that NEC-4 fixes a problem in NEC-2 that

* This work was performed under the auspices of the U. S. Department of Energy by the University of California, Lawrence Livermore National Laboratory under Contract No. W-7405-Eng-48.

resulted in inaccurate results for wires with changing radius. NEC-2 is not accurate for either a single step in wire radius or a tapered change over several segments. NEC-4 is much more accurate in most cases of changing wire radius.

The matrix evaluation routines in NEC-4 have been rewritten to make them more stable for low frequencies. The single precision NEC-4 can be used in many cases where NEC-2 would fall apart. However, we still run most problems in double precision, since it gives more confidence and computers usually have enough memory. I do not know of any studies on the solution stability for single precision for models of 10,000 or more segments, where the reduced storage would really be important.

NEC-4, in the LLNL version, still does not have dynamic array allocation, but array dimensions are set in a parameter file. It is easy to change array sizes, but you need a Fortran compiler, or I will try to compile for sizes that are requested. There are also some new or modified commands, such as a catenary wire, an improved helix command and more control of the range of segments affected by GM. CM or CE commands for text can be used anywhere in the input file. Voltage sources and one or more incident plane waves can be combined for excitation. LE and LH commands have been added to compute near E and H along linear paths. They can be combined to evaluate line integrals of E or H along piecewise-linear paths. For large problems that cannot fit into RAM, NEC-4 uses a single direct-access file for the matrix where NEC-4 needed four copies of the matrix in sequential-access files.

NEC-4 remains a wire modeling program with a limited capability for modeling surfaces with the MFIE. It will not be of use for many currently important problems of modeling microstrip patch antennas or dielectric bodies. If anyone has questions not answered on the IPAC website they can contact me at burke2@llnl.gov or phone 925-422-8414.

Modular Development of CAE Models for Lossy Matching Networks: Part I

Shaohua Li, Perry Wheless

Abstract—We consider here fundamental computer-based models for the multimode behavior of single-layer helical air-core RF inductors at frequencies up to approximately 1.5 GHz. Four specific CAE models are presented, with discussion of their merits and limitations. This study is one in a series, motivated by the desire to improve practical design and analysis of efficient antenna tuning units, power amplifier tank circuits, and other RF applications employing helical air-core RF inductors.

Index Terms—Antenna tuning units, RF inductors, inductor CAE, electronic component models.

I. INTRODUCTION

Antenna design projects often include the design of a companion antenna tuning unit (ATU) to match the transmitter and transmission line characteristic impedance to the impedance(s) presented at the antenna element feed point(s). For moderate to high operating power levels at frequencies from LF (30 - 300 kHz) up into the UHF (300 MHz - 3 GHz) region, the fundamental ATU subsystems to achieve phase and power division control are networks comprising three reactive components. RF inductors and capacitors are typically configured in Tee or Pi circuits, and radio system engineers generally are aware how they can scientifically determine three L and C values that will match an arbitrary (finite) complex load impedance Z_L to a desired real input impedance Z_0 at a specific design frequency, and simultaneously provide a desired phase shift in the process. RF power amplifiers similarly have tuned (tank) circuits involving both inductors and capacitors. ATU and amplifier tank circuit losses are always in the background consciousness of design engineers, and losses may be significant, but typical circumstance is that the designer lacks the computer-aided engineering (CAE) tools for an accurate and reliable analysis of the network losses. This article is the first in a series, which will culminate in the computer-based tools to thoroughly characterize such networks, including losses, in practical applications.

Achievement of the objective of useful CAE software is an evolutionary project which, of course, is predicated on beginning from correct fundamental principles and appropriate engineering models. The starting point, therefore, is an examination and modeling of the essential characteristics and behavior of the helical air coils and variable plate capacitors typically found in ATUs and tank circuits. This paper reports some highlight results from first studying RF inductor basics.

The authors are with the Department of Electrical and Computer Engineering, University of Alabama, Tuscaloosa, AL. E-mail: li022@bama.ua.edu.

II. ILLUSTRATIVE CASE STUDY

To enable quantitative treatment of RF inductor behavior, a specific (but typical) helical air coil is discussed. To facilitate some comparisons to [1], we here adopt a coil of the same dimensions, namely, 12.9 single-layer turns of 18-gauge copper wire with the following nominal dimensions: an inside solenoid radius of $a_i = 0.248$ inches, mean radius of the solenoid $a = 0.268$ inches, axial length $c = 0.89$ inches, and pitch $\Psi = 0.041$. When the inductor is horizontally mounted above a ground plate, the S_{21} transmission characterization, as measured in manual mode by a Hewlett-Packard 8505A vector network analyzer, is shown in Figure 1. This data closely emulates that given in [1], with individual data points marked by small circles. We parenthetically note that excellent interpolation of values between the measurement points is available in MATLAB [2] by use of the *interp1* function with the ‘pchip’ (piecewise cubic Hermite interpolation) option. The *interp1* function was utilized in generation of the solid line plots in Figure 1.

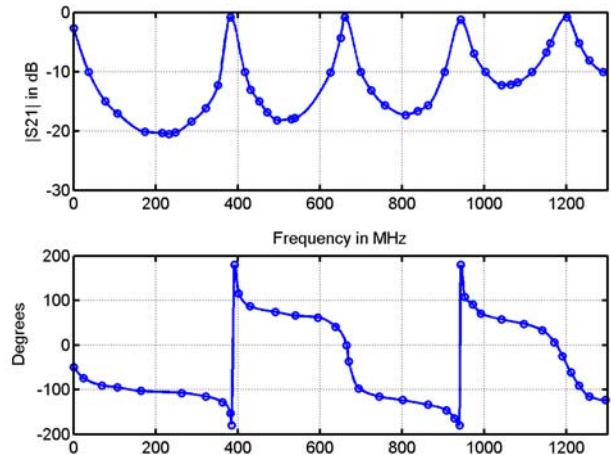


Fig. 1. S_{21} of horizontally mounted RF inductor.

Figure 1 straightaway shows a behavior pattern that may be surprising to some RF design engineers. The “classic model” for a real-world RF inductor, which is the subject of the next section, clearly indicates that, at sufficiently high frequency, the device will be self-resonant. RF circuit designers are well-aware of the reality of that resonance effect, and carefully avoid it in requirements such as, for example, an RF choke in the bias circuit of a high-power tube amplifier. The surprise, at least for some, is that real RF inductors exhibit not just one, but multiple resonances, as frequency is increased.

Experimental characterization, illustrated by Figure 1, is more useful as a guide to appropriate models for RF inductors than as a routine design aid. Engineers are inclined by their training to develop and work with models, and justifiably so, because accurate and reliable models may be used and extended to new and various circumstances, versus the rigid limitation that measured data is obtained under constrained and quite specific conditions. In short, good engineering models offer a high degree of flexibility and convenience. In the following sections, we will discuss a series of basic models that are all amenable to computer implementation as a CAE tool. Through application to the same "case study" inductor, the objective is for the reader to acquire a good sense of the relative power and limitations of each model.

III. CLASSIC MODEL

The so-called "classic" model, widely depicted in undergraduate electrical engineering textbooks on circuit theory and basic electronics, is shown in Figure 2. Rhea [1] is a good reference for a summary review discussion of the classic model. From only a casual consideration of Figure 2, one can quickly and correctly conclude that this will be a low-frequency model of limited general utility, and so we restrict our discussion of the classic model here.

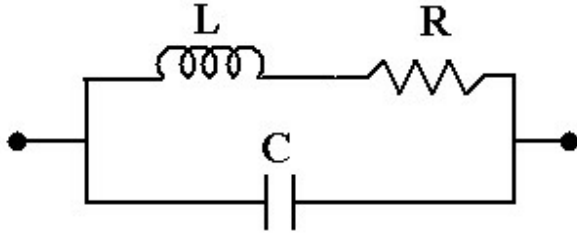


Fig. 2. Classic model of an RF inductor.

Wheeler [3] developed an almost exact low-frequency (i.e., quasi-static) classic inductor model that requires the calculation of complete elliptic integrals. An approximation formula which does not require elliptic integrals, but is accurate at low frequencies to approximately 1% for coil lengths greater than 0.67 times the radius, is

$$L = \frac{n^2 a^2}{9a + 10c} \simeq 1 \mu H \quad (1)$$

with $n = 12.9$ T, $a = 0.268$ inch, and $c = 0.890$ inch. Medhurst [4] gives the capacitance relationship

$$C \text{ (in pF)} = H \times D \implies C \simeq 0.65 \text{ pF} \quad (2)$$

where $D = 2a$ (in cm) and H is a function of $\frac{c}{2a}$, the length-to-diameter ratio. Please see [4] or Table 1 of [1] for how H is obtained from $\frac{c}{2a}$.

$$\frac{c}{2a} = \frac{0.89}{2 \times 0.268} = 1.6604 \implies H = 0.48 \quad (3)$$

The estimation of R starts with the relation for unloaded Q [4]

$$Q_u = 0.15 a \varphi \sqrt{f_0} \quad (4)$$

with f_0 in units of Hz and φ is determined from its relation to $\frac{c}{2a}$ and $\frac{d_w}{s}$ (the fraction of axial length c occupied by wire) in accordance with Table 2 of [1]. Here, $\frac{d_w}{s} = 0.58$ for 18-gauge copper wire, giving $\varphi \simeq 0.72$ and

$$Q_u = 0.15 \times (0.268 \times 0.0254) \times 0.72 \times \sqrt{f_0} \quad (5)$$

and, finally,

$$R = \frac{\omega L}{Q_u} = \frac{2\pi f_0 L}{Q_u}. \quad (6)$$

Since R is a function of frequency, it is calculated as a vector inside the MATLAB modeling program.

To enable the classic model to show its best possible predictions in comparison to the measured data, two low-frequency ranges were selected and, also, the MATLAB modeling program performed a least squares optimization of the nominal numerical values of R , L , and C via the function *lsqcurvefit* provided in the MATLAB package. The graphical result for $|S_{21}|$ for the restricted frequency range 1 to 50 MHz (in steps of 1 MHz) is in Figure 3, where it is evident that the optimized parameter values of $L = 1.0619 \mu H$ and $C = 0.65349$ pF improve on the original model fit. The low-frequency (static) classic model is moderately successful in predicting the actual experimental data up to a frequency of 50 MHz.

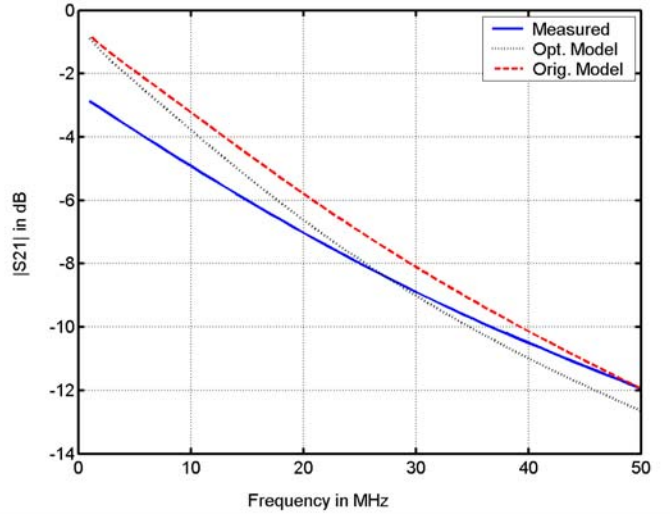


Fig. 3. Classic model vs measured, 1-50 MHz.

However, when we just extend the frequency range of interest to 1 - 300 MHz, still far from the full range of 1 - 1300 MHz, the classic model already exhibits breakdown (see Figure 4). It is immediately clear that this elementary model is not even a candidate for the multimode reality shown in Figure 1. It is visually difficult to discern if the optimized classic model is actually better than the original classic model in Figure 4, so we introduce a quantitative measure of error at this point.

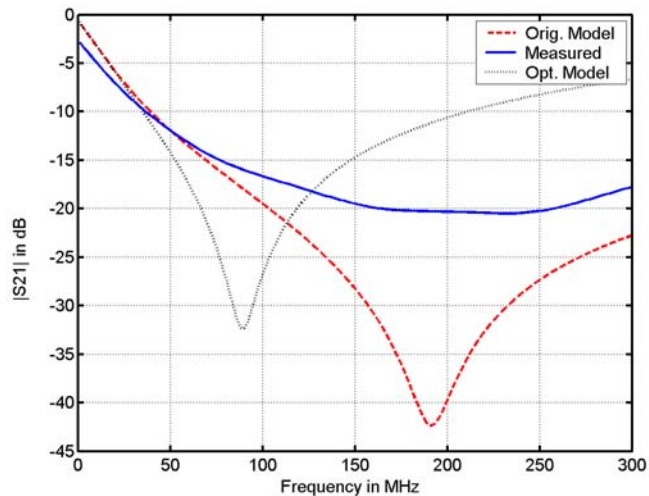


Fig. 4. Classic model vs measured, 1-300 MHz.

IV. QUANTIFICATION OF MODEL ERROR

In this paper, the measured data is taken as the standard reference, and the various model predictions are then compared to the experimental data. The measure of model discrepancy is then the “SSE” (sum of the errors squared). For all modeling cases reported here, the frequency step is 1 MHz. Therefore, comparing the results for two different models with 1-300 MHz results presented is direct and immediate, without the need for additional manipulation or interpretation. When the frequency span is different, some interpretation is necessary. To facilitate comparisons in those instances, the total SSE is divided by the number of points at which the composite calculation was made, yielding an SSE_{avg} value *per point*.

The observant reader will quickly note that the original measurement points depicted in Figure 1 are not in 1 MHz steps, and wish to know the procedure applied in the event a frequency for analysis does not exactly match one of the original measurement frequencies. In those cases, the standard value for model accuracy comparison is determined by interpolation between the nearest original measured data points in MATLAB using the *interp1* function with ‘pchip’ option, as previously discussed.

Using this error quantification technique, the 1-50 MHz classic model result of Figure 3 has a $|S_{21}|$ error of $SSE = 136.83$ ($SSE_{avg} = 2.74$ per point) for the original component values, and $SSE = 66.92$ ($SSE_{avg} = 1.34$ per point) for the least squares optimized component values. For the 1-300 MHz classic model result of Figure 4, the original values give $SSE = 24,685$ ($SSE_{avg} = 82.3$ per point) and the optimized components yield modeling error $SSE = 22,451$. ($SSE_{avg} = 74.8$ per point) Hence, the optimized classic model curve in Figure 4 really is a better fit to the measured curve than that of the original classic model.

V. TRANSMISSION LINE MODEL

A new multimode model for the helical air-core RF inductor was proposed in 1997 in [1]. In this model, the inductor is

replaced with a section of transmission line of electrical length Θ degrees and characteristic impedance Z_0 , as indicated in Figure 5. In Figure 1, we note that $|S_{21}|$ has its first local minimum just above 200 MHz, and then makes its first return approach to 0 dB at approximately 383 MHz. The response at 383 MHz suggests that the appropriate transmission line length at this frequency is 180° .

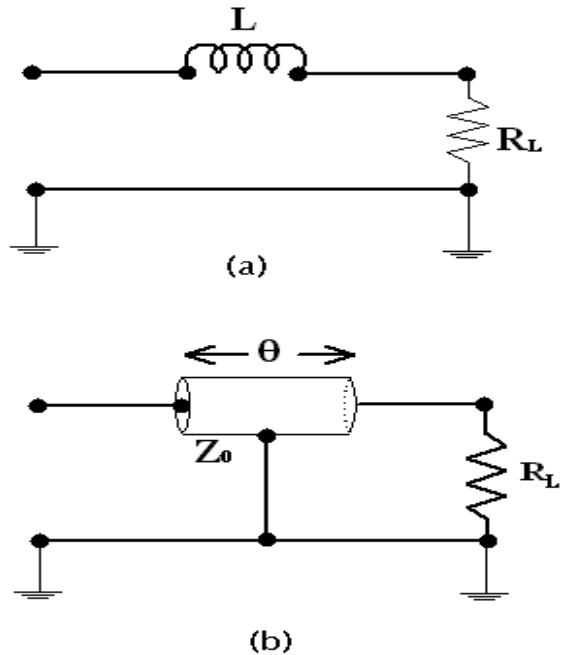


Fig. 5. Transmission line model.

A computer-aided implementation again aids our appreciation of the essential merit of this particular model. Two instructive results are included here. In both cases, the MATLAB program was allowed in each case to apply the *lsqcurvefit* function in order to optimize the values of line length and Z_0 to provide the best possible fit against the measured data. Figure 6 shows model performance from 1 to 395 MHz in 1 MHz steps:

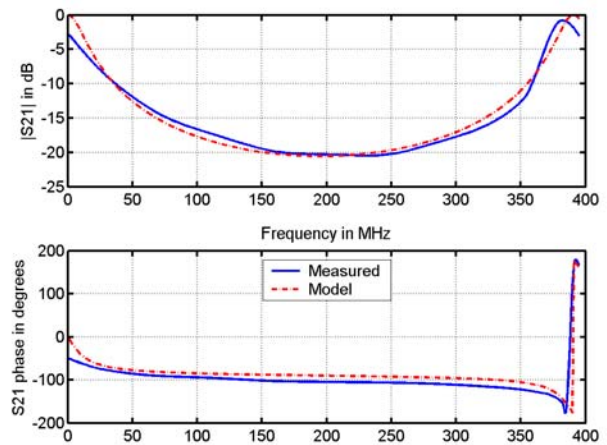


Fig. 6. Transmission line model, 1-395 MHz.

The modeling error calculations associated with Figure 6 are $SSE |S_{21}| = 415.5$, or $SSE|_{avg} = 1.052$ per point, and $SSE \angle S_{21} = 2.42 \times 10^5$, or $SSE \angle_{avg} = 614.5$ per point. It was deemed desirable, for illustration and comparison purposes, to capture the first inductor “resonance” in the frequency range of examination, although this choice clearly adversely affected the SSE result for the phase angle to a significant degree. For the full 1-1300 MHz range of measured data is modeled, the result is Figure 7.

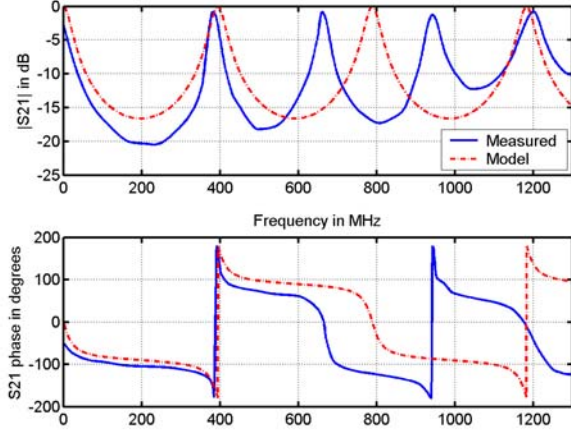


Fig. 7. Transmission line model, 1-1300 MHz.

As one would expect, the transmission line section has precisely periodic repetitions of its fundamental behavior. Figure 7 emphasizes that the higher frequency resonances of the real-world RF inductor, on the other hand, are not at integer multiples of the fundamental frequency. The modeling error calculations associated with Figure 7 are $SSE |S_{21}| = 48596$, or $SSE|_{avg} = 37.4$ per point, and $SSE \angle S_{21} = 1.646 \times 10^7$, or $SSE \angle_{avg} = 1.27 \times 10^4$ per point. One is led by these two results to conclude that the transmission line model can be a quite effective tool at low to medium frequencies (below the first resonance, here about 383 MHz), but its range of validity does not extend to the higher-frequency regime.

VI. HELICALLY CONDUCTING SHEET MODEL

In this section, we first present (and then extend in the next section) results using a multimode RF inductor model recently advocated by Mezak [5]. This model considers the RF inductor to be a helically conducting sheet which has both TM (transverse magnetic) and TE (transverse electric) modes and exhibits dispersion. It is especially accurate in predicting the resonant frequencies of an inductor. The key governing equations were first developed in studies on helical line models for the traveling-wave tube community in the 1960s. One of the better references for finding full details of the original derivation steps is Pierce [6]. A concise description of the calculational process, for a given frequency, follows.

First, the transcendental equation

$$(\gamma a)^2 \frac{I_0(\gamma a) K_0(\gamma a)}{I_1(\gamma a) K_1(\gamma a)} = (\beta_0 a \cot \Psi)^2 \quad (7)$$

(where $\gamma^2 = \beta^2 - \beta_0^2$, a = radius of the inductor helix, I_0 and I_1 are the modified Bessel functions of the first kind of order 0 and 1, respectively, K_0 and K_1 are the modified Bessel functions of the second kind of order 0 and 1, respectively, β_0 = propagation constant in free space, β = propagation constant of the helix, and Ψ = the helix pitch angle) is solved for γ . Then the value of β follows from the relation $\gamma^2 = \beta^2 - \beta_0^2$. The so-called transverse characteristic impedance of the helix is next found from the relation (see [6], page 30)

$$K_t = F_1 \cdot F_2 \quad (8)$$

where factor F_1 is

$$F_1 = \left(\frac{\gamma}{\beta}\right)^2 \left(\frac{\beta}{\beta_0}\right) \left[\frac{120 I_0^2}{(\gamma a)^2}\right] \quad (9)$$

and

$$F_2 = \left[\left(1 + \frac{I_0 K_1}{I_1 K_0}\right) (I_1^2 - I_0 I_2) + \left(\frac{I_0}{K_0}\right)^2 \left(1 + \frac{I_1 K_0}{I_0 K_1}\right) (K_0 K_2 - K_1^2) \right] \quad (10)$$

Choosing to use the regular chain (ABCD) matrix \tilde{T} instead of the normalized chain matrix \tilde{T}_n , we directly take

$$Z = K_t. \quad (11)$$

Z_0 is the system characteristic impedance (typically 50Ω). Z , in turn, allows determination of the regular chain matrix elements from the well-known form for a section of transmission line

$$\begin{bmatrix} A & B \\ C & D \end{bmatrix} = \begin{bmatrix} \cos(\beta \ell) & jZ \sin(\beta \ell) \\ \frac{j}{Z} \sin(\beta \ell) & \cos(\beta \ell) \end{bmatrix} \quad (12)$$

where it should be noted that the inductor length, previously denoted c , is here denoted by ℓ . Here, the load resistor R_L in Figure 5 is equal to the system characteristic impedance Z_0 , and complex S_{21} is found from

$$S_{21} = \frac{2}{A + \frac{B}{R_L} + C R_L + D}. \quad (13)$$

For short, the helically conducting sheet model will be referred to as simply the *Mezak model*. To show how the dispersion model predicts the multiple resonant frequencies rather well, the model is compared to the measured data over the full 1 - 1300 MHz range in Figure 8. On the other hand, as Figure 8 shows, this model is less successful in emulating, both qualitatively and quantitatively, the S_{21} data in between the multiple resonant frequencies.

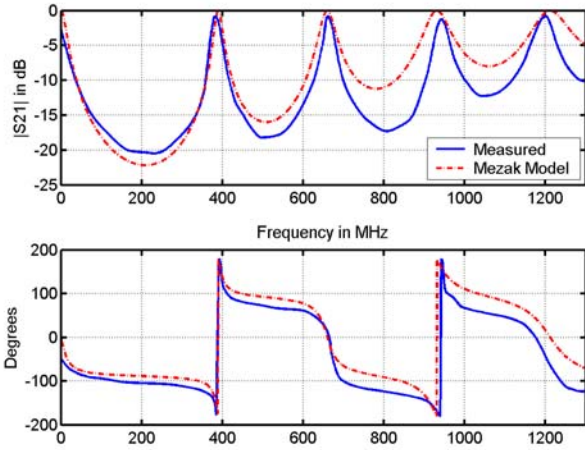


Fig. 8. Mezak model, 1 - 1300 MHz.

VII. EXTENDED HELICAL CONDUCTING SHEET MODEL

In applied electromagnetics, a frequent occurrence is that theoretical values for a real operational device are related to experimental measurement values through a fractional linear transformation. For example, in the context of antenna feed-point impedances, see [7]. Motivated by favorable prior experiences, an empirical study was made of extending the so-called Mezak model to include a fractional linear transformation of the form

$$Z_m = \frac{a_1 Z_i + a_2}{a_3 Z_i + 1} \quad (14)$$

with Z_m representing measured data at a specific frequency and Z_i representing the corresponding ideal, or theoretical, value (in this case, the value from the Mezak model). The procedure for determining the complex constants a_1 , a_2 , and a_3 is detailed in [8]. The extended model is here called the Transformed model. A more formal name has not been chosen because the investigative study is not yet complete, and the model details remain subject to further evolutionary change.

Three results for different frequency spans are presented in Figures 9, 10, and 11 below. Data row 1 in Table I (for 1 - 200 MHz) indicates the notable extent to which the Transformed model is superior to the Mezak model in the low-frequency regime, below the first inductor resonance. Indeed, the Transformed model is the best performer in the low-frequency regime of all the models discussed in this paper. For very wide frequency ranges (see data row 3 in Table I), the Transformed model offers modest improvement over the Mezak model, although a span of 1 to 1300 MHz obviously overextends the range of validity for both.

It should be noted that there are special circumstances that result in performance degradation of the present Transformed model implementation. An example is modeling the subject RF inductor over the frequency range 1 to 395 MHz. The resonance at approximately 383 MHz actually causes the Transformed model, in its present form, to degrade the input data received from the Mezak model (see data row 2 in Table I). Work

continues toward anticipating and eliminating such anomalous behavior for this model.

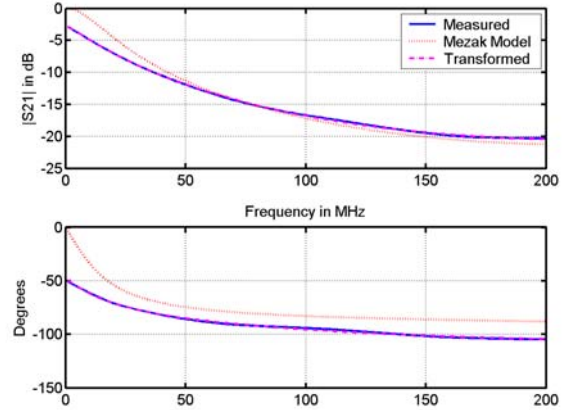


Fig. 9. Transformed model, 1-200 MHz.

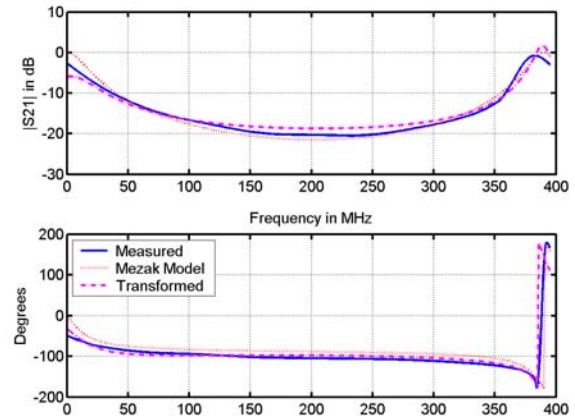


Fig. 10. Transformed model, 1-395 MHz.

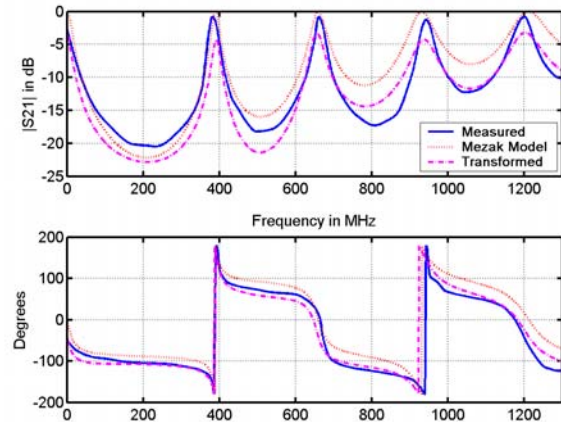


Fig. 11. Transformed model, 1 - 1300 MHz.

TABLE I
Error Comparison of Mezak and Transformed Models

Range (MHz)	Mezak $SSEs$		Transformed $SSEs$	
	$ S_{21} $	$\angle S_{21}$	$ S_{21} $	$\angle S_{21}$
1 - 200	304	5.15e4	1.94	106
1 - 395	523	2.65e5	705	2.43e5
1 - 1300	1.66e4	2.45e6	7907	2.32e6

VIII. CONCLUSIONS

Antenna engineers concerned with the design of antenna phasing and power divider networks would like computer software that provides more accurate and reliable CAE of the RF inductors and capacitors used in such practical systems. RF circuit design engineers charged with the production of high-power amplifiers share the desire of their antenna system counterparts. The ultimate objective of our work is such a computer software product, which we intend to make available in the public domain.

It is important for all radio engineers to be cognizant of the multimode behavior of real RF inductors, and aware that the widely accepted "classic model" for helical air-core coils is severely limited in its scope of applicability. Another fundamental realization of significance about RF inductors, not discussed here, is that the dominant capacitance associated RF coils is not turn-to-turn (interwinding) capacitance as long assumed, but rather the distributed capacitance with respect to ground. Reference [1] has a clear discussion of this point, and interested readers should see the *Additional Remarks* section of that paper.

This report has presented some highlight features of four RF inductor models: the classic model, the transmission line model, the so-called Mezak model, and the Transformed model incorporating a fractional linear transformation. Evidence and results examined during the course of this study first suggested that the distributed inductance and capacitance associated with inductors for RF applications made a (TEM) transmission line section a viable model candidate at sufficiently low frequencies. Later, measured inductor behavior above the first resonance of the coil then revealed that a waveguide (that is, TE/TM) model, with dispersion, becomes more appropriate at higher frequencies. The approach of [5] is based on a non-TEM, dispersive helix, and provides good predictions of inductor resonant frequencies. Because the Mezak model does not incorporate loss in its formulation, it is generally deficient in emulation of the behavior of $|S_{21}|$ and S_{21} phase away from the near neighborhoods of resonances. Work to date by the authors with the Transformed model is encouraging, and how it may accurately account for the losses associated with real-world RF inductors is being actively studied. Continuing efforts are also underway to determine if a variation of the fractional linear transformation will allow development of an even better, more comprehensive RF inductor model.

REFERENCES

[1] Rhea, Randall W., "A multimode high-frequency inductor model," *Applied Microwave & Wireless*, November/December 1997, pp 70-80.
 [2] MATLAB is a registered trademark of The MathWorks, Inc., 3 Apple Hill Drive, Natick, MA 01760 – 2098.

[3] Wheeler, H.A., "Inductance formulas for circular and square coils," *Proc. IEEE*, vol. 70, pp 1449-1450, 1982.
 [4] Medhurst, R.G., "H.F. resistance and self-capacitance of single-layer solenoids," *Wireless Engineer*, February 1947, pp 35-43 and continued March 1947, pp 80-92.
 [5] Mezak, John A., "Modeling helical air coils for wireless and RF applications," *RF Design*, January 1998, pp 77-79.
 [6] Pierce, J.R., *Traveling-Wave Tubes*, New York: D. Van Nostrand Company, Inc., 1950, Chapter III and Appendix II.
 [7] Kajfez, Darko and Dube, Rene L., "Measurement of impedance transformation on practical dipoles," *IEEE Trans. Antennas and Propagation*, July 1973, pp 544-549.
 [8] Kajfez, Darko, "Numerical determination of two-port parameters from measured unrestricted data," *IEEE Trans. Instrumentation and Measurement*, vol. IM-24, no. 1, March 1975, pp 4-11.

CEM CODE VALIDATION USING INFRARED THERMOGRAMS

John Norgard

Electromagnetics Laboratory
Department of Electrical & Computer Engineering
College of Engineering & Applied Science
University of Colorado
P.O. Box 7150
Colorado Springs 80933-7150
USA

Keywords: Infrared, Thermograms, Electromagnetic, Microwave, Metrology, Correlation, Code Validation, Radiation, Scattering, Waveguide/Cavity Modes

Abstract

In this article, an infrared (IR) measurement technique is presented that has been developed to measure electromagnetic (EM) fields. This technique uses a minimally perturbing, thin, planar IR detection screen to produce a thermal image (e.g., an IR thermogram) of the intensity of the EM energy over the two-dimensional region of the screen. Several examples are presented using this thermal technique to measured EM fields. These examples include:

- i) radiation from microwave sources
- ii) scattering from conducting bodies
- iii) coupling through apertures in shielded enclosures.

These examples illustrate the use of this thermal technique to correlate theoretical data with experimental observations. This technique has also been used to experimentally validate complicated numerical codes that predict electric field distributions in areas where conventional hard-wired probes would significantly perturb the fields being measured, for example inside waveguides and cavities (E-Fields) and near apertures. Surface current distributions (H-Fields) on metallic surfaces also can be measured with this technique.

INTRODUCTION

A non-destructive, minimally perturbing infrared (IR) measurement technique has been developed to observe electromagnetic (EM) fields. Metallic surface currents and charges also can be measured with this technique.

This IR measurement technique produces a two-dimensional IR thermogram of the electric or magnetic field being measured, i.e. a two-dimensional gray-scale image of the measured temperature profile in the screen. After calibration, the temperature data can be presented as a two-dimensional isothermal contour map or a three-dimensional relief map of the intensity of the EM field incident on the screen.

The IR measurement technique has been applied to determine:

- a. The radiated fields from microwave antennas and high-power microwave (HPM) sources, e.g. near-field intensities and far-field antenna patterns of horn antennas [1];
- b. Diffraction patterns of EM fields scattered from complicated metallic objects [2,3];
- c. Intensities of EM fields coupled through apertures in shielded enclosures [4]; and
- d. Modal distributions of EM fields excited inside cavities [5,6].

Electric and magnetic fields can be measured separately. Examples are presented of the thermal images of electric field distributions

- radiated from microwave horn antennas
- coupled through apertures
- induced inside waveguide cavities (internal cylindrical cavity modes).

Examples of magnetic field distributions near conductive surfaces and induced surface currents on metallic surfaces have also been taken.

The advantages and disadvantages of this new IR measurement technique are also discussed.

IR MEASUREMENT TECHNIQUE

The IR measurement technique is based on the Joule heating that occurs in a lossy material as an EM wave passes through the material. A thin, planar sheet of a lossy carbon loaded paper or a carbon loaded polyimide film are used to map electric fields; a thin, planar sheet of a lossy ferrite loaded epoxy is used to map magnetic fields. In either situation, the absorbed heat energy is converted into conducted and convected heat energy and into re-radiated EM energy. The radiated EM energy is concentrated in the IR band. This "black body" energy is detected with an IR (Scanning) Array or with an IR (Staring) Focal Plane Array (FPA).

IR Experimental Setup

This technique involves placing a lossy, non-perturbing IR detection screen near the source of the EM energy in the plane (or planes) over which the field is to be measured.

Electromagnetic Parameters. The detector screen is made from a thin sheet of linear, homogenous, and isotropic lossy material. From the complex form of Poynting's Theorem for a linear, homogeneous, and isotropic material, the absorbed power P_{abs} within the given volume V of the lossy material is a function of the electric (E) and magnetic (H) field intensities inside the screen and is given by

$$P_{abs} = \int_V (\sigma E^2 + \omega \varepsilon'' E^2 + \omega \mu'' H^2) dv \quad (1)$$

where σ is the conductivity of the detector screen, ε'' is the imaginary component of the permittivity (dielectric constant) of the detector screen, μ'' is the imaginary component of the permeability of the detector screen, and ω is the radian frequency of the incident field. The volume integral is over the illuminated portion of the detector screen. The spectral characteristics of the complex constitutive parameters

$(\mu, \varepsilon, \sigma)$ must be known (or measured) over the entire frequency bandwidth of interest in the measurements.

Electric and magnetic field detector screens have been designed and fabricated to be sensitive to only one component of the magnitude of the electric or magnetic fields, as discussed below.

The incident EM energy is absorbed by the lossy material and is converted into thermal heat energy, which causes the temperature of the detector material to rise above the ambient temperature of the surrounding background environment by an amount that is proportional to the local electric and/or magnetic field intensity (energy) at each point (pixel) in the screen material. In regions where the field is strong, the absorbed energy is large and the resulting pixel temperatures are high; in regions where the field is weak, the absorbed energy is small and the resulting pixel temperatures are low. The resulting two-dimensional temperature distribution over the surface of the screen is detected, digitized, and stored in the memory of the IR camera.

The temperature distribution on the surface of the screen without any EM energy incident on the screen is also stored in the memory of the IR camera as an ambient background reference temperature distribution. The difference in the temperature at each pixel location between the illuminated and the non-illuminated screens is a result of only the effects of the electric or magnetic field incident on the screen at each pixel location. These EM effects can be visualized by presenting the differenced two-dimensional temperature profile as a false color image, where cool colors (for example shades of blue) represent weak areas of EM energy and hot colors (for example shades of red) represent strong areas of EM energy. The resulting two-dimensional false color image is called an IR thermogram, i.e., an iso-temperature contour map, and is a representation of the electric and/or magnetic electric field distribution passing through the screen material.

Thermal Parameters. For a planar sheet of detector material supported by a block of non-conducting material, i.e., a styrofoam block, the thermal heat transfer problem reduces to considering only the radiative and convective heat losses from the front surface of the detector material.

The convective heat loss h_{conv} is approximated by

$$h_{conv} = h_o (T - T_{amb})^{1.25} \quad [W / m^2] \quad (2)$$

where h_o varies between 1.4 and 1.6, depending on the detector screen material.

The radiative heat loss h_{rad} is approximated by

$$h_{rad} = \varepsilon_{IR} \sigma_{IR} (T^4 - T_{amb}^4) \quad [W / m^2] \quad (3)$$

where ε_{IR} is the detector surface emissivity (not to be confused with the electric dielectric constant ε), σ_{IR} is the Stefan-Boltzman constant in $W / m^2 K^4$ (not to be confused with the electric conductivity σ).

The conductive heat loss h_{cond} is negligibly small, and is approximated by

$$h_{cond} \cong 0 \quad [W / m^2] \quad (4)$$

In the above equations, all temperatures are in degrees Kelvin.

Thermal Equilibrium. The heat transfer problem in the detector material involves solving a non-linear, second-order differential equation in both space and time, while considering radiative and convective (negligible conduction) heat losses from the surface of the material, conductive heat transfer inside the material, and EM power absorption in the material as a function of distance into the material. For the case of the thin detector screens considered here, the transverse temperature distribution is initially considered to be constant in the axial direction normal to the surface of the material, so that the conductive term normal to the surface of the screen can also be ignored and the power absorbed can be considered independent of the direction normal to the surface of the screen. Also, the time dependence of the absorbed heat energy can be ignored for the steady-state solution that follows.

Relating the convective, conductive, and radiative heat losses in equations (2) and (4) to the absorbed power in equation (1), results in the following equation at thermal equilibrium:

$$P_{abs} \cong h_{rad} + h_{conv} + \underbrace{h_{cond}}_{\cong 0} \quad (5)$$

For a properly optimized detector screen, thermal equilibrium is achieved in just a few seconds.

This non-linear thermal/electrical equation can be solved for the temperature T of the detector material, as a function of the incident electric and or magnetic field, using approximate techniques to solve Maxwell's Equations (Snell's Laws and Fresnel's Laws) and the Heat Equation for a plane wave incident on a four layered (air/screen/insulator/air) planar film of lossy material in thermal equilibrium. This solution can then be inverted numerically for the incident electric or magnetic field intensity as a function of the screen temperature. The inverted result is then fitted with a high-order polynomial to yield a calibration curve (formula) for the detector screen material.

The theoretical solution was verified experimentally at NIST/Boulder. A calibrated standard gain horn was used to irradiate the screen with a precisely known near-field intensity (at the surface of the screen). The intensity of the field was increased, from initial detection to final saturation of the difference temperature. At each intensity, the IR camera was used to measure the resulting surface temperature (color) of the screen. A "color" table of temperature verse incident field strength was developed, which agreed well with the theoretically derived results discuss above. A simple table-look-up scheme can then be used to convert temperature into field intensity. Approximately 30 dB of dynamic range is available in the thermal technique when a scanning array is used as the IR detector and approximately 40 dB of dynamic range is available when a FPA is used.

Approximate Solution

Equation (5) is a highly non-linear equation for large temperature variations above ambient, due to the thermal processes of convection and radiation. However, for small temperature variations of only a few tenths of a degree above ambient, equation (5) can be linearized for small incremental temperature changes $\Delta T = T - T_{amb}$ above the ambient temperature T_{amb} .

This condition of small temperature variations above ambient is a desirable operational constraint, because this is also the requirement for small absorption of the

EM energy passing through the screen, which equates to small perturbations of the incident field to perform the measurement. For this minimally perturbing measurement case, an almost direct linear correlation exists between the incremental surface temperature ΔT and the electric or magnetic field intensity. For this ideal case, a sensitive IR camera is required. In addition, the constitutive parameters of the IR detector screen are optimized to produce a large temperature rise in the detector material for a small amount of absorbed energy.

For the Focal Plane Array (FPA) used to make the IR thermograms presented in this paper, temperature differences as small as $\Delta T = 9$ mK can be detected.

Care is, therefore, exercised in the selection of the screen material not to significantly perturb the electric or magnetic field by the presence of the lossy material. The screen is designed to absorb from 1% to 5% of the incident power and to produce a temperature change of less than a few degrees.

Electric and magnetic fields produced by continuous wave (CW) sources operated in the sinusoidal steady-state mode are easy to measure because of the large amount of energy contained in the wave. Transients produced by High-Power Microwave (HPM) pulsed sources, especial repetitively pulsed sources, can also be measured if the average energy content in the pulse is high enough to raise the temperature of the detector screen above the minimum temperature sensitivity of the IR camera. The thermal mass of the detector screen holds the absorbed energy long enough to capture the IR thermogram of the pulse.

IR Detector Screen

Referring to equation (1), the detector screen material is tailored to respond to only one component of the field, e.g. by optimizing the values of the electrical conductivity σ and the imaginary part ϵ'' of the permittivity of the screen material relative to the imaginary part μ'' of the permeability of the material, the detector screen can be made sensitive to either the tangential component of the electric field or the tangential component of the magnetic field in the plane of the screen.

For example, an *electric* field detector screen can be constructed either i) from a lossy material with high

conductivity σ and low imaginary permittivity ϵ'' and low imaginary permeability μ'' or ii) from an electrically polarizable material with high imaginary permittivity ϵ'' and low conductivity σ and low imaginary permeability μ'' .

Alternatively, a *magnetic* field detector screen can be constructed from a magnetically polarizable (magnetizable) material with high imaginary permeability μ'' and low conductivity σ and low imaginary permittivity ϵ'' .

The optimization of the thermal and electrical parameters of the detection screen material is guided by an electromagnetic/thermal (EMT) computer code based on a plane wave obliquely incident on a planar interface between air and the lossy detector screen material. Other absorptive and re-emittive transducing materials [7-9] have been studied for use as passive thermal screens for infrared scene discrimination. In the examples that follow, only the electric field detector is considered in this article.

Electric Field Detector Screen. For the detection of electric fields, the IR detection screen can be made from a thin, planar sheet of carbon paper (e.g., Teledeltos Paper) or a carbon loaded polyimide film (e.g., Kapton). The detector screen used to make the electric field thermograms presented in this article has a conductivity of 8 mhos/meter and is 80 μm thick. This material is non-polarizable and non-conducting; therefore, the imaginary components of the permittivity ϵ'' and the permeability μ'' are negligibly small. For this conducting, non-polarizable, non-magnetic detector screen material, maximum heating occurs due to the electric field and negligible heating occurs due to the magnetic field.

For plane waves normally incident on this carbon loaded electric field detection screen and for an IR FPA with a temperature sensitivity as small as 9 mK, electric fields with a magnitude on the order of 61.4 V/m (1 mW/cm² of incident power) can be easily detected. This result was obtained empirically from experimental data in which the incident power level was incrementally decreased until no electric field contours were discernable on the IR thermogram from the ambient background level.

IR Camera

The temperature difference between the detector screen material and the background is detected, digitized, and stored in the memory of an IR camera on a pixel by pixel basis. The FPA system used for this article has 256 by 256 pixels per frame of data. Each pixel is an Indium Antimonide (InSb) IR photo detector operated in a photo-voltaic mode. The array operates at liquid Nitrogen temperatures and is enclosed in a dewar.

IR Images

The stored thermal data represents the temperature distribution over the extent of the detector screen and is a map (image) of the intensity of the electric or magnetic field distribution absorbed in the screen. For small temperature rises less than a few degrees, the electric and magnetic field intensities are nearly linearly proportional to the temperature change.

Spatial Resolution. The spatial resolution of the IR thermogram is a function of the number of pixel elements in the FPA and is fixed by the angular resolution of the wide angle, normal, or telephoto lens used on the IR camera when taking the IR image. The telephoto lens can be used to look at small details of the field structure on the detector screen; the wide angle lens can be used to look at large scale trends in the field structure on the detector screen.

The telephoto lens also has the added advantage for regular field mapping applications of allowing the IR camera to be located a long distance away from the object under test, and, thus, removing any perturbing effects that the metallic structure of the camera might have on the field distribution being measured.

Thermal Resolution. The thermal resolution of the IR thermogram is a function of the digitizer in the FPA. The FPA used to take the IR thermograms presented in this article uses a 12 bit digitizer. For a 12 bit digitizer, the temperature range seen by the IR camera is divided into 256 increments. Each digitized increment is assigned a unique color, resulting in a temperature resolution of 256 color levels.

Thermal Errors. The resulting IR image of an EM field depends on the combined EM and thermal properties of the detector material and is subject to several small and controllable errors.

Lateral Conduction Effects. Conductive heating in the transverse direction within the screen material causes thermal "blurring" from the hot spots on the screen to nearby cold spots. This thermal blurring tends to fill in the nulls (minimums) somewhat, whereas, the areas of maximum heating (peaks) are not effected very much by this effect. This effect can be minimized by operating at small temperature variations above ambient.

Lateral Convective Effects. Convective heating of the top of the screen due to heat rising from the bottom of the screen causes the top of the screen to appear slightly hotter than the bottom of the screen. This thermal "bleeding" of the image can be kept to a minimum by operating at small temperature variations above ambient. This bleeding effect can be eliminated completely by placing the IR detector screen in a horizontal position and observing the image with the IR camera looking down on the screen from above or from the side using an IR mirror.

IR Measurement Accuracy

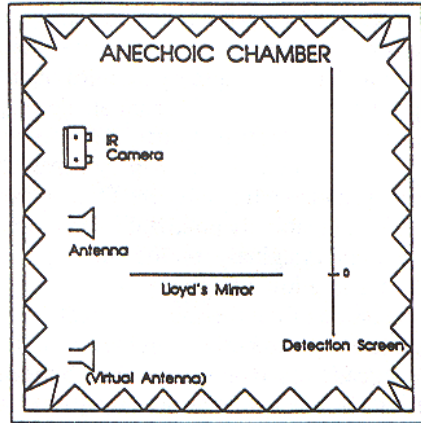
The accuracy of the IR measurement technique can be demonstrated by performing a simple experiment with a known theoretical solution. In this experiment, as shown in *figure 1*, the diffraction pattern from "Lloyd's Mirror" was measured.

In the Lloyd's mirror experiment, the resulting diffraction pattern is caused by the antenna interfering with its image in a large ground plane. The second peak in *figure 1* is smaller in magnitude than the first peak because the radiation pattern of the horn antenna used in the experiment decreases with angle from the bore sight direction of the horn. The near-field (Fresnel Zone) antenna pattern of the horn antenna was used to obtain the theoretical results.

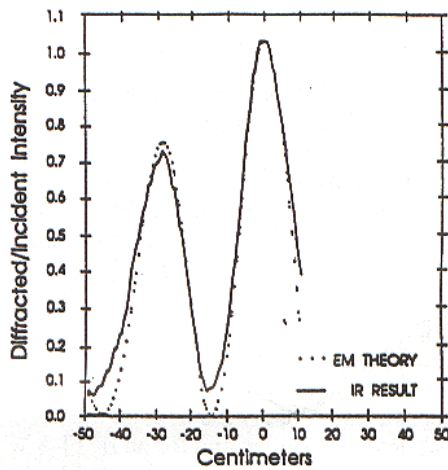
The screen material was optimized to measure only the tangential component of the electric field intensity in the plane of the screen.

This experiment was performed in an anechoic chamber, as shown in *figure 1a*. Good correlations between theory and experiment were obtained, as shown in *figure 1b*. The worst errors occurred in the minimums (deep nulls) of the diffraction patterns were thermal blurring from the surrounding hot areas tended to obscure the real depth of the minimums. Some thermal blurring out of the maximums into the surrounding areas also occurred, obscuring the real height of the maximums.

Even with conductive blurring and convective bleeding of the image, the measurement error is less than approximately 10% under normal controlled test conditions.



(a)



(b)

Figure 1. “Lloyd’s Mirror” experiment (an antenna near a large ground plane) – correlation between theory and experiment: (a) IR experimental setup (looking down into the anechoic chamber) and (b) near-field diffraction pattern from a finite ground plane (along a horizontal line through the center of the IR detection screen).

IR Advantages and Disadvantages

The IR measurement technique provides a quick and accurate method to observe EM fields in a two-dimensional plane. However, only the magnitude of

the electric or magnetic field is measured; no phase information is detected. Also, since this technique is based on the thermal mass of a detector material, high energy is required to produce good thermal images of EM fields.

IR THERMOGRAMS

Some examples of measured IR thermograms of electric fields are presented below.

IR Thermograms of Electric Fields

Radiation from a Horn Antenna, and Scattering from and Coupling into a Cylinder

As an example of the IR measurement of electric fields, a right circular cylinder, containing a long, thin slot aperture in its side, was irradiated with a plane EM wave from a pyramidal horn antenna. IR thermograms were made of the radiation pattern of the horn, the diffraction pattern of the EM field scattered from the cylinder, and the cylindrical modes excited inside the cavity. The experimental setup is shown in *figure 2*.

Aperture Coupling into a Finite Cylinder. The experimental cylinder is one meter in length and has an inner diameter of approximately 10 centimeters. The rectangular slot aperture is 64 millimeters in width and is 10 centimeters in length. The slot is located in the middle of the cylinder and is oriented parallel to the axis of the cylinder. The cylinder is irradiated with microwave energy at 3 GHz (10 centimeter wavelength) from a pyramidal horn antenna, polarized in the circumferential direction of the cylinder. Cylindrical TE modes are predominantly excited by the wave polarization inside the cavity.

A large IR detector screen of carbon paper was positioned in the transverse radial plane that intersected the middle of the slot aperture. Another IR disk was positioned inside the cylinder in the same cross-sectional plane.

Experimentally obtained IR thermograms of the results are shown in *figures 3 through 5*. The brightness of each color in the image corresponds to the intensity of the EM field. The radiation pattern of the horn, the diffraction patterns of the EM fields scattered from the cylinder, and the modal patterns of the induced cylindrical cavity modes are clearly indicated in these figures.

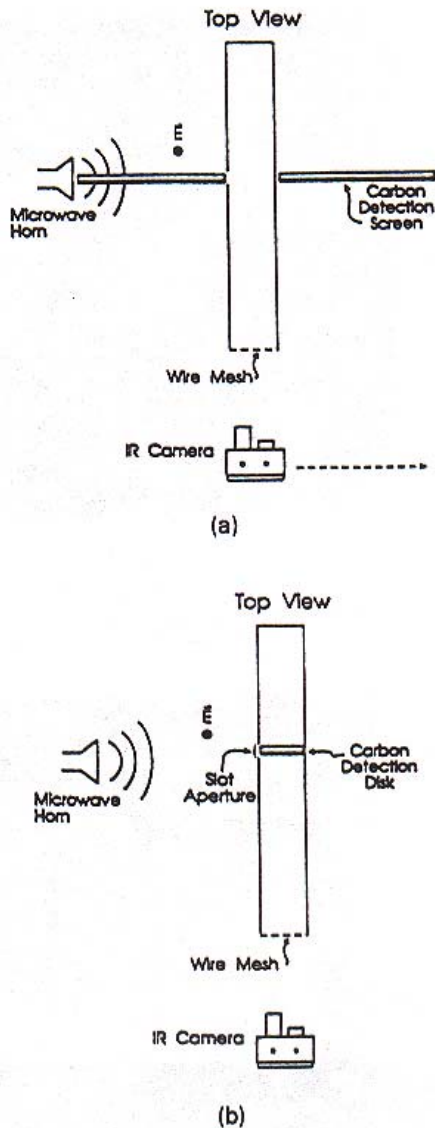


Figure 2. Experimental arrangement for IR images of plane wave scattering from a finite-length cylinder and slot aperture coupling into a cylindrical waveguide cavity. (a) IR camera and detector screen setup for measuring exterior scattered fields. (The IR camera is positioned on either side of the cylinder.) (b) IR camera and detector screen for measuring interior cylindrical waveguide cavity modes. (The IR camera is positioned on the axis of the cylinder and looks through a wire mesh screen simulating a microwave shield – microwave opaque, optically transparent).

Thermograms of the incident microwave field of the pyramidal horn antenna are shown in *figure 3*. *Figure 3(a)* is an image of the electric field traveling wave in the longitudinal plane in front of the horn. *Figure 3(b)* is an image of the electric field in the transverse near-field plane one meter in front of the aperture of the horn. Thermograms of the field scattered from the cylinder are shown in *figure 4*. *Figure 4(a)* is the image of the electric field standing wave created between the horn and the cylinder. This thermogram shows the interference pattern between the incident wave and the scattered cylindrical wave. *Figure 4(b)* is an image of the electric field traveling wave in the shadow zone of the cylinder. The null behind the cylinder and the diffracted wave off the top and bottom of the cylinder can be seen in this thermogram. Thermograms of the induced modes coupled into the cylindrical cavity are shown in *figure 5*. *Figure 5(a)* is an image of the electric field coupled through the aperture for a frequency 10% below the cutoff frequency of the cylindrical waveguide. The EM energy coupled through the aperture is visible in this thermogram and, as expected, has the radiation pattern of an electric dipole. The dominant TE_{11} waveguide modal pattern is partially developed in the center of the waveguide. *Figure 5(b)* is an image of the electric field coupled through the aperture for a frequency 10% above the cutoff frequency of the cylindrical waveguide. The dominant TE_{11} waveguide modal pattern is now fully developed in the center of the waveguide.

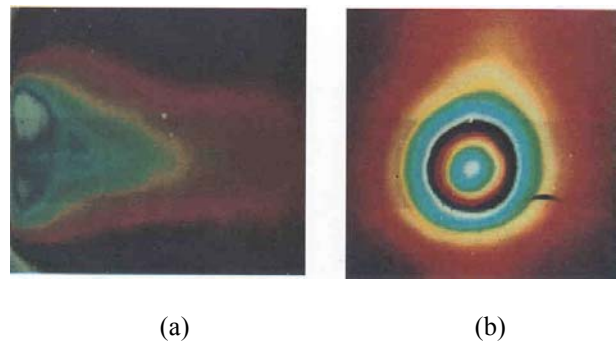


Figure 3. IR thermograms of a microwave horn radiation pattern (a) in the longitudinal plane (in the vertical plane through the center of the horn aperture and (b) in the transverse plane (a cross-sectional cut of the microwave beam 1m in the near field in front of the aperture plane).

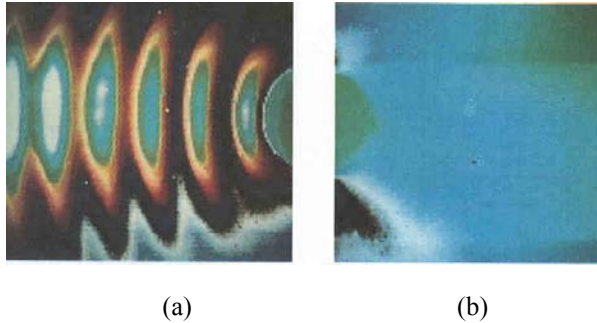


Figure 4. IR thermograms of the diffraction pattern of the scattered electric field from a finite cylinder: (a) standing wave between the horn and the cylinder (showing the constructive and destructive interference patterns between the incident and reflected waves) and (b) traveling wave behind the cylinder (showing the shadow zone behind the cylinder and the surface diffracted waves).

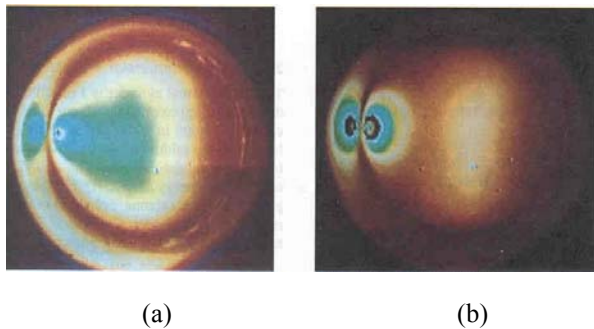


Figure 5. IR thermograms of the excited cylindrical waveguide cavity mode inside the cylinder (the long, thin horizontal slot aperture is located in the center of the left-hand side of the IR thermograms - note the reflection in the walls of the waveguide - parallax effect): (a) excitation of an evanescent mode (at a frequency 10% below cutoff) and (b) excitation of the dominant TE_{11} cylindrical waveguide mode (at a frequency 10% above cutoff - note the dipole pattern at the aperture, as predicted by Bethe hole coupling theory).

In the above thermograms, note that the IR camera used to take the thermograms was one of the early models of a FPA Staring array and the IR detector screen was made from a Kapton film. The thermograms shown are the original raw data directly off the camera. The white spots are bad pixels, which were easily removed using a simple nearest neighbor averaging scheme. In addition, for an easy test setup, the thermograms were taken with a vertical detector screen. The distortion of the image

(which should be symmetrical - top to bottom) caused by thermal bleeding of the extra heat from the bottom to the top of the picture is clearly seen in thermogram 3(b). This is eliminated when using a horizontal screen. Finally, note that the black horizontal mark to the lower right of center in thermogram 3(b) is a mechanical flaw (non-uniformity in surface conductivity) in the Kapton film, which was later processed out of the digital image.

CEM Code Validation

A scale model of a F16 aircraft was made. A 1/64th plastic scale model was spray-painted with several coats of silver paint to make it conductive. The scale model was cut into the carbon screen so that the wings of the airplane were in the plane of the paper. This scale model was illuminated by a horn antenna at different frequencies, angles of incidence, and polarizations. The screen was also moved into a transverse plane through the middle of the wings of the aircraft and the process repeated. The experiment was performed inside the anechoic chamber at the Air Force Research Laboratory at the Phillips Research Site (AFRL/PRS). The test setup is shown in figure 5 for the test case of normal incidence with the screen in the plane of the wings. The resulting IR thermogram is shown in Figure 6. Note the standing wave setup in front of the aircraft between the incident spherical wave from the horn antenna and the reflected wave from the nose of the aircraft. The transparent radome is not included in the model of the aircraft; however, the radome, which houses the Fire Control Radar (FCR), is included in the model. A surface wave has also developed on both sides of the aircraft between the nose of the aircraft and the missile rails on the wing tips. Diffraction off the trailing edge of the wingtips is evident in the thermogram, as is the shadow zone behind the aircraft.

A similar numerical study of the F16 was done at the Air Force Research Laboratory at the Rome Research Site (AFRL/RRS) using the *General Electromagnetic Model for the Analysis of Complex Systems (GEMACS)* code on a full size F16 aircraft. The code was run on a CRAY computer at Los Alamos National Laboratory (LANL). The numerical results were compared to experiments performed on the aircraft at the "upside down" Air Force facility at the Newport test site.

The results from the numerical code are presented in Figures 7 and 8. Figure 7 is a map of the surface currents on the aircraft; figure 8 is a picture of the scattered fields. The experimental results from the IR

measurements compare well to the numerical results from the *GEMACS* code. Note that the (*GEMACS*) code was run with a plane wave incident on the aircraft, whereas, in the measurements, the source produced a spherical wave in the far field at the location of the model.

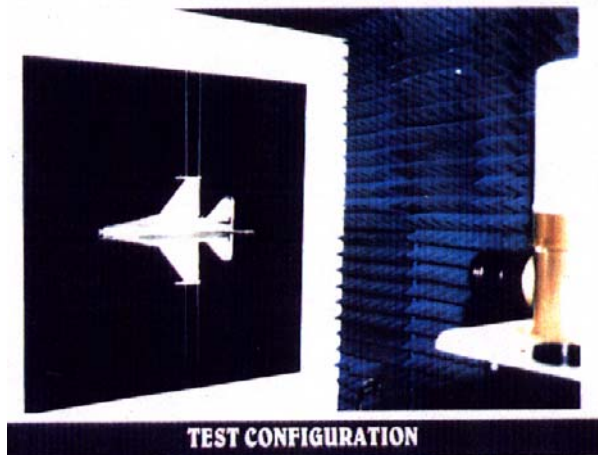


Figure 5. Test setup for scale model F16. Normal incidence in the plane of the wings.

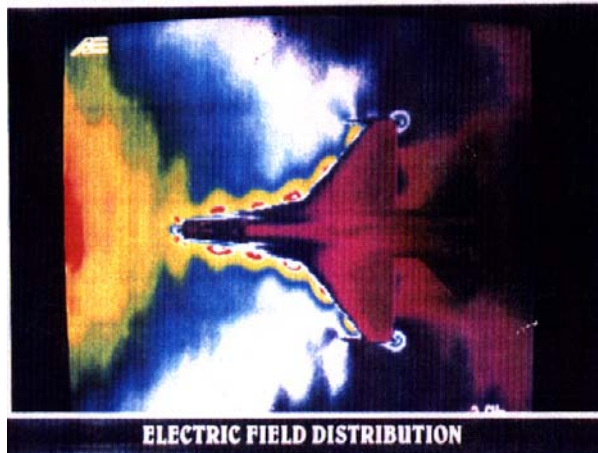


Figure 6. Test results for scale model F16. IR thermogram for normal incidence in the plane of the wings.

CONCLUSION

The IR measurement technique is a viable method to aid in the determination of EM fields radiated from antennas, scattered from complex metallic objects, and coupled into complex cavity structures. This method is of particular importance in the study of scattering

objects with complicated geometrical shapes, whose field patterns may not be found easily using theoretical methods.

The IR method allows for rapid observation of EM field activity and interference, resulting in an in-depth understanding of the EM radiation, scattering, and coupling phenomena. Qualitative and quantitative comparisons can be made between the fields measured using the thermal radiation experimental approach and the fields predicted using a theoretical/numerical approach. Experimental and theoretical data, therefore, can be easily correlated with this technique.

Test results similar to those reported here have been used in the past to validate other numerical codes [10,11].



Figure 7. F16 surface currents from the *GEMACS* code.



Figure 8. F16 scattered fields from the *GEMACS* code.

ACKNOWLEDGEMENT

The author would like to acknowledge the help and support of this IR project from his colleagues Carl Stubenrauch at NIST/Boulder, Mike Harrison, Bill Prather, Hugh Pohle, and Joe Sadler at the Microwave Research Laboratory at the USAF Phillips Laboratory and Jerry Genello and Steve Lapree at the EM Vulnerability Laboratory USAF Rome Laboratory.

REFERENCES

- [1] D.W. Metzger, J.D. Norgard and R.M. Sega, "Near-Fields Patterns from Pyramidal Horn Antennas: Numerical Calculation & Experimental Verification" *IEEE-EMC Transactions*, Vol. 33, No. 3, August 1991, pp. 188-196.
- [2] R.M. Sega and J.D. Norgard, "Infrared Measurement of Scattering and Electromagnetic Penetrations through Apertures," *IEEE-NS Transactions*, Vol. NS-33, No.6, December 1986, pp. 1858-1883.
- [3] J.D. Norgard, R.M. Sega, K.J. Ianacone, M.G. Harrison, A.T. Pesta and M.A. Seifert, "Scattering Effects of Electric and Magnetic Field Probes," *IEEE-NS Transactions*, Vol. NS-36, No. 6, December 1989, pp. 2050-2057.
- [4] R.M. Sega and J.D. Norgard, "An Infrared Measurement Technique for the Assessment of Electromagnetic Coupling," *IEEE-NS Transactions*, Vol. 32, No. 6, December 1985, pp. 4330-4332.
- [5] R.M. Sega, J.D. Norgard and G.J. Genello, "Measured Internal Coupled Electromagnetic Fields Related to Cavity and Aperture Resonance," *IEEE-NS Transactions*, Vol. NS-34, No. 6, December 1987, pp. 1502-1507.
- [6] J.D. Norgard, D.C Fromme and R.M. Sega, "Correlation of Infrared Measurement Results of Coupled Fields in Long Cylinders with a Dual Series Solution," *IEEE-NS Transactions*, Vol. NS-37, No. 6, December 1990, pp. 2138-2143.
- [7] W.H. Purdy and W.E. Woehl, "A Passive Thermal Screen for Infrared Scene Simulation," *Optical Engineering*, Vol. OE-15, No. 6, December 1976, pp. 554-558.
- [8] V.T. Bly, "Passive Visible to Infrared Transducer for Dynamic Infrared Images Simulation," *Optical Engineering*, Vol. OE-21, No. 6, December 1982, pp. 1079-1082.
- [9] M.J. Scholl, "Thermal Considerations in the Design of a Dynamic IR Target," *Applied Optics*, Vol. 21, No. 4, February 1982, pp. 660-667.
- [10] R.W. Ziolkowski and J.B. Grant, "Scattering from Cavity Backed Apertures: The Generalized Dual Series Solution of the Concentrically Loaded E-Pol Slit Cylinder Problem," *IEEE-APS Transactions*, Vol. AP-13, No. 5, May 1987, pp. 504-528.
- [11] R.W. Ziolkowski, W.A. Johnson and K.F. Casey, "Applications of Reimann-Hilbert Problem Techniques to Electromagnetic Coupling through Apertures," *Radio Science*, Vol. 19, No. 6, November-December 1984, pp. 1425-1431.

Review of Advanced Electromagnetic Modeling Techniques in the Computer Code FEKO based on the Method of Moments with Hybrid Extensions

Ulrich Jakobus

EM Software & Systems GmbH
Otto-Lilienthal-Str. 36, D-71034 Böblingen, Germany
E-Mail: u.jakobus@emss.de

Abstract — The aim of the present tutorial is to introduce some advanced electromagnetic modeling techniques based on the Method of Moments (MoM) with various hybrid extensions. We are using the computer code FEKO [1] as a reference, and illustrate in the following several extensions that have been made in FEKO to the classical MoM in order to allow an efficient and fast analysis of a variety of complex electromagnetic radiation and scattering problems. The aim is not to go too much into the technical details (for the interested readers suitable references will be given), but rather to present an overview only, with a few selected application examples.

1 Introduction

Today it is no longer possible to imagine being engaged in antenna design or solving EMC problems without the help of computer modeling. These tools have evolved to an indispensable aid for engineers by not only complementing measurements, but at the same time reducing the number of such measurements, and as a consequence resulting in faster design cycles and reduced costs (just to give one example, a single RCS or antenna radiation pattern measurement of a ship in the open sea is quite expensive).

A variety of such computational methods exist for the numerical solution of Maxwell's equations. These include for instance FDTD (finite difference time domain), FEM (finite element method), MoM (method of moments), TLM (transmission line matrix method), PEEC (partial element equivalent circuit) and many more. It is beyond the scope of this tutorial to give a comprehensive overview of these techniques and to discuss the advantages or disadvantages of each. Some material can be found in Refs. [2–4] and in many other books and review papers.

Depending on the specific problem under consideration (such as time versus frequency domain, metallic object or highly heterogeneous material, closed structure or open radiation problem, low or high frequency etc.) some of the available numerical techniques might be more suitable than others. There is no method which can claim to be the best. Thus we believe that the future belongs to hybrid methods, where several different numerical techniques are combined in order to use the most suitable solver for a specific part of a problem.

In the following we focus on the frequency domain MoM with various extensions. The MoM has been developed originally by Harrington [5], and has since been extended by numerous research groups around the world to a mature and powerful technique.

This paper is organized as follows: The MoM is briefly introduced in Section 2, both for metallic and dielectric scattering problems. Then several options to solve high frequency problems within the MoM framework are discussed in Section 3, namely current- and ray-based hybrid methods, but also fast integral equation techniques.

2 Classical Method of Moments

2.1 Metallic objects

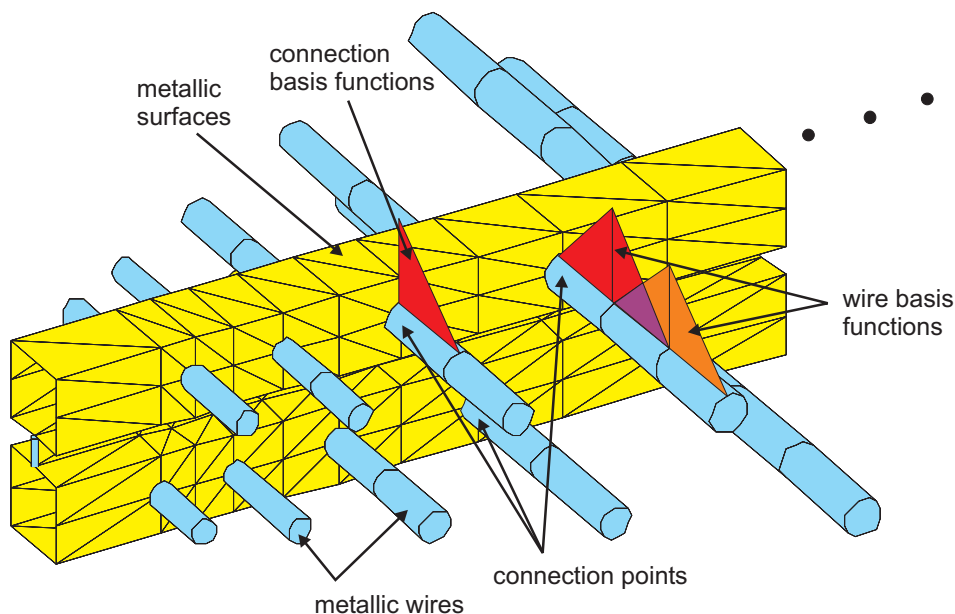


Fig. 1: General representation of a meshed region for the MoM consisting of surfaces and wires.

A general metallic object consisting of metallic wires and surfaces is shown in Fig. 1. This specific structure is part of a logarithmic periodic antenna, but the following discussions are very general and independent of the actual shape.

Metallic wires are discretized into electrically short (i.e. short as compared to the wavelength) wire elements, so-called segments. As indicated in Fig. 1, we are using overlapping triangular basis functions g_n to model the line current I along wires:

$$I = \sum_{n=1}^{N_I} \beta_n \cdot g_n \quad (1)$$

Likewise, on the metallic surfaces we are using a triangular mesh, and to represent the electric surface current density \vec{J} , the well known Rao Wilton Glisson rooftop basis functions \vec{f}_n are used [6], also known as CN/LT (constant normal, linear tangent) [4]. One obtains

$$\vec{J} = \sum_{n=1}^{N_J} \alpha_n \cdot \vec{f}_n \quad (2)$$

with unknown expansion coefficients α_n .

In general, one must also make provision for a current flow from wires to surfaces, so called wire / plate junctions. Special basis functions need to be considered there, which are more or less one half basis function g_n on the wire (maximum current at the connection point) and a singular (with respect to the surface current density \vec{J}) behavior on the plate. Further details shall be omitted here, the interested reader is referred to [7–11]. Our implementation is similar to [11] and [12], with some modifications.

Within the MoM framework the unknown expansion coefficients α_n in eqn. (2) and β_n in eqn. (1) are obtained by means of solving a system of linear equations with $N = N_J + N_I$ unknowns. For electrically large structures, N will be large, and thus both memory requirement for the matrix of the system of linear equations (scaling with N^2) as well as the run-time for the solution (scaling typically with N^3 for direct solvers) might be prohibitive. Ways to overcome this problem will be discussed in Section 3.

The system of linear equations results from applying certain boundary conditions. For perfectly conducting objects we are using the electric field integral equation (EFIE) based on

$$\vec{E}_{tan} = \vec{E}_{s,tan} + \vec{E}_{i,tan} = 0 \quad (3)$$

with the scattered (s) and impressed (i) contributions. Explicit expressions for the scattered fields as a function of the sources I and \vec{J} shall be omitted here, they can be found elsewhere (e.g. [13–15]).

We are using the EFIE due to the generality of its application also to open bodies. The alternative formulations MFIE (magnetic) and CFIE (combined) offer advantages: The MFIE is more robust and stable since it is based on a Fredholm integral equation of the second kind, and thus for instance iterative techniques converge faster, and the CFIE in addition to this lower condition number is also more robust with respect to internal resonances. However, both MFIE and CFIE require the bodies to be closed, which is not the case for many practical problems.

Thus we have to use the EFIE in these cases. This is not really a problem, since numerous studies have shown an excellent stability also at resonances, and the relatively high condition number can be dealt with by using either robust direct solvers based on an LU-decomposition with double precision accuracy, or when iterative techniques are required like for the MLFMM (multilevel fast multipole method) then good preconditioners have to be developed (for instance an incomplete LU-decomposition with a small level of fill-in).

In order to show the application of the MoM to metallic bodies, just one simple example shall be presented here: Scattering from a brass strip with dimensions 63.6 mm tall, 6.3 mm wide, and

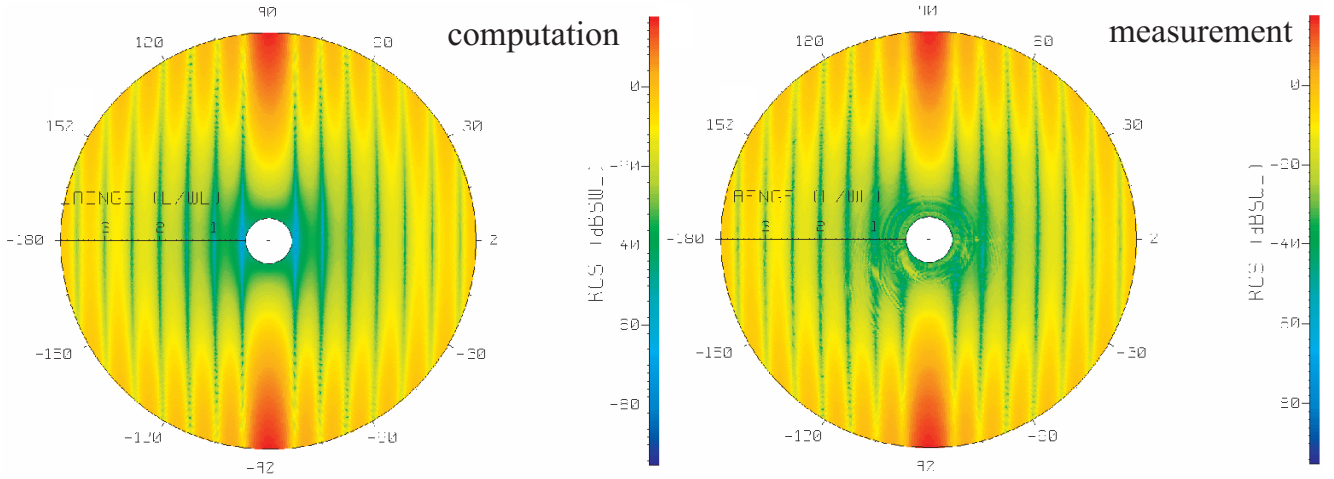


Fig. 2: Computed (left) and measured (right) RCS of a brass strip as a function of the observation angle in the far-field and the frequency (radial direction).

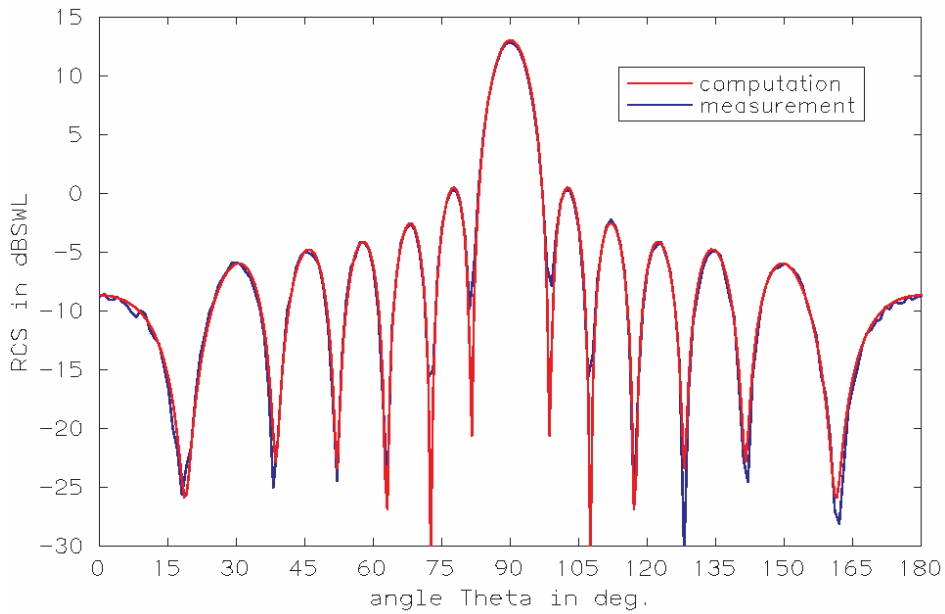


Fig. 3: Comparison of measured and computed RCS for one specific frequency of 15 GHz.

0.32 mm thick. In Fig. 2 we see on the left hand side the computed RCS, as a function of the far-field angle (also angle in the graph) and as a function of the frequency (in radial direction we have length of the strip normalized to the wavelength, l/λ). The graph to the right shows the measured RCS, these highly accurate measurements have been taken from [16, 17].

One sees some small irregularities for the measured data around the center due to measurement errors, but otherwise measured and computed results are in very close agreement. This is confirmed by a quantitative 2-D plot for one single frequency: Fig. 3 shows the RCS for a fixed frequency of 15 GHz (i.e. $\lambda = 20$ mm, then circle in Fig. 2 with a fixed radius $l/\lambda = 63.6/20 = 3.18$). Also this result of RCS versus angle shows a very good agreement.

2.2 Dielectric bodies

Though not the main focus of this paper, for the sake of completeness it shall be mentioned that the MoM is also very well suited for the treatment of dielectric / magnetic bodies (also lossy). The author has compiled another review paper on this topic, see [18], and thus here the main techniques shall be mentioned only:

- Surface equivalence principle for partly homogeneous regions: Here equivalent electric and magnetic surface current densities \vec{J} and \vec{M} , respectively, are introduced at the interfaces between different media. Different integral formulations are possible, we focus on the PMCHW technique [13, 19].
- Volume equivalence principle for inhomogeneous bodies. This is based on a 3-D volumetric discretization of the material (as opposed to FEM or FDTD not of the surrounding air). But due to the dense nature of the MoM matrices this technique typically results in big matrices, and a FEM/MoM hybrid method might be the preferred approach for solving highly inhomogeneous scattering problems.
- Special Green's function techniques for selected geometries only. We support this in FEKO for layered spherical bodies [20] and planar multilayer substrates [21]. The latter has efficient far-field approximations, and sophisticated interpolation strategies for a fast evaluation of the occurring Sommerfeld integrals. In principle, this Green's function method can be used for any geometry where Maxwell's equations can be solved analytically, also cylindrical or ellipsoidal structures.
- Special formulations applicable to selected configurations only, but highly accurate and in particular very efficient, see e.g. the treatment of dielectrically coated wires as described in [18], or also the thin dielectric sheet formulations which the MoM offers (e.g. for glass windows of a car).

Further details and in particular many more references to original papers can be found in [18]. Similar to metallic bodies, also one example shall be presented here for the dielectric bodies. Fig. 4 shows the analysis of a planar inverted F antenna (PIFA) in the 1.8 GHz mobile phone range. The solid line without symbols indicates the effective gain in the horizontal plane, if the mobile phone radiates in free space. The two lines with the symbols show the reduction in effective gain due to power loss in the hand, if the hand is included in the model at two different positions partly covering the antenna.

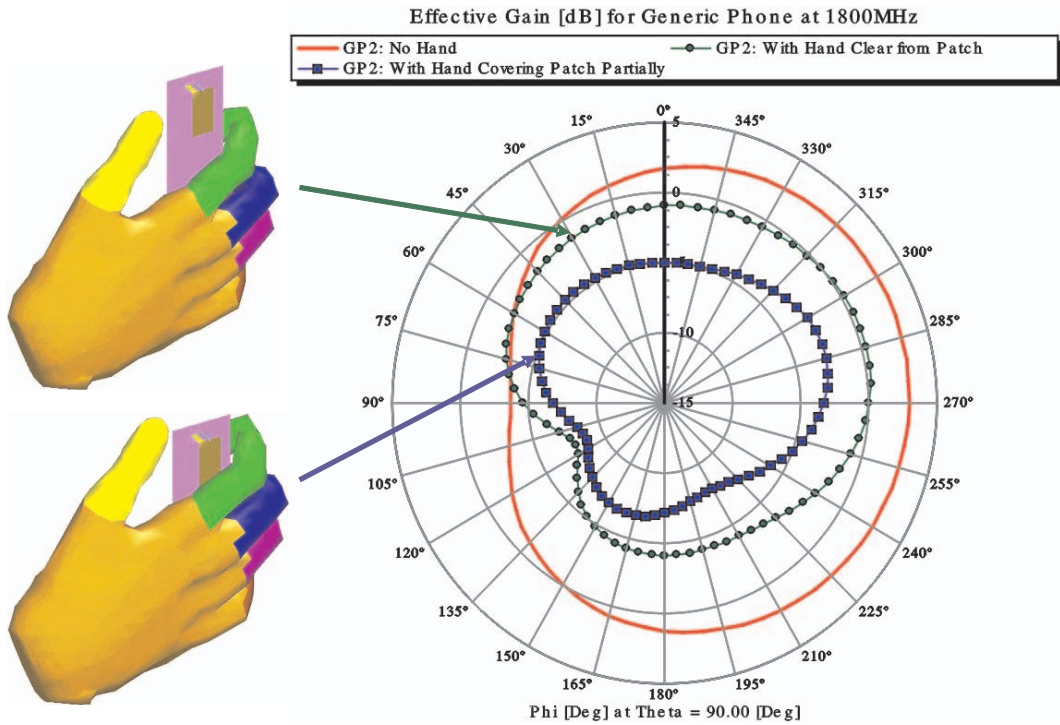


Fig. 4: Influence of the hand on the radiation characteristics of a mobile phone.

3 Solution of high frequency problems

3.1 General considerations

We have seen in Section 2 that for the MoM we need to discretize into electrically small elements (triangular patches, wire segments), and that we end up with N unknowns that need to be determined from the solution of a dense complex system of linear equations.

If we consider the aircraft example in Fig. 5, then for a frequency of 100 MHz we require a mesh of 20 337 metallic triangles, resulting in $N = 30319$ basis functions (each basis function is associated with an edge between two triangular patches). Using double precision accuracy with 16 Bytes for one complex number, the memory requirement for the MoM matrix is $16 \text{ Bytes} \cdot N^2 = 13.7 \text{ GByte}$.

This is quite large, but not a problem for any modern computer system, in particular if one supports (like FEKO does) parallel processing in connection with efficient out-of-core solver techniques. With an out-of-core solver, one can even solve this structure on a simple notebook computer with the traditional MoM (provided there is enough hard disk space of course).

However, one runs into serious trouble when the frequency is higher than the 100 MHz here. If we only double the frequency, then for 2-D surface meshes, N is already four times larger, and the memory requirement scales with N^2 , i.e. then 16 times larger (219 GByte). Trying to solve the aircraft with the traditional MoM at 1 GHz would require approximately 134 TByte, which makes any solution impossible.

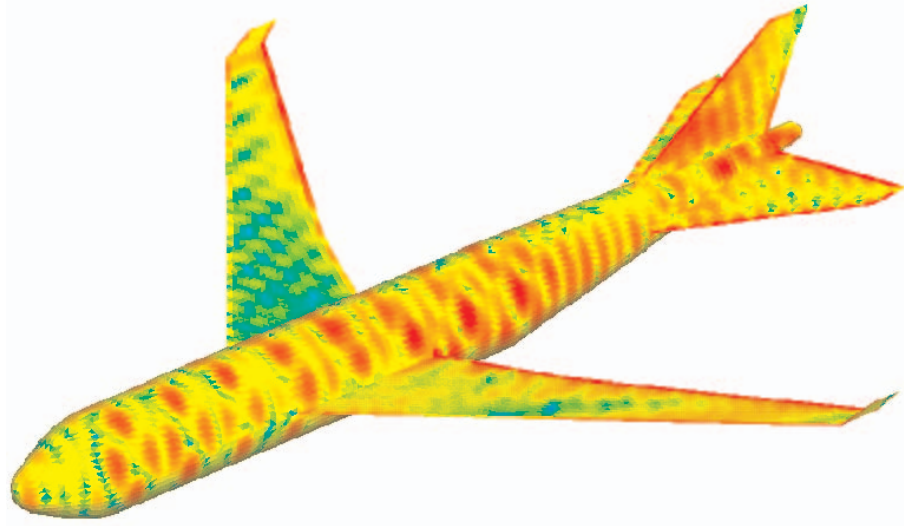


Fig. 5: Model of an aircraft with surface current density when illuminated by an external antenna of the navigation system at 100 MHz.

Alternative techniques have to be used, either by switching to fast integral equation methods, or by using a combination of the MoM with asymptotic high frequency methods. These shall be discussed in the following.

3.2 Current based hybrid method

The MoM is a current based technique: In eqn. (2) we approximate the surface currents \vec{J} by the linear superposition of basis functions with unknown coefficients α_n . The main problem is that within the MoM formulation we need to solve a system of linear equations in order to obtain these N coefficients.

The idea for the current based hybrid method can be illustrated with the help of Fig. 6: Still everywhere currents are introduced, which are unknown in the first place. They are also again expressed as the linear superposition of basis functions with unknown coefficients as in eqn. 2. But the main difference as compared to the MoM is that the expansion coefficients α_n for the currents J^{asym} in the asymptotic region are not determined by solving a system of linear equations, but they are obtained directly by means of high frequency approximations.

The simplest such approximation is Physical Optics (PO), where the asymptotic currents are defined as

$$\vec{J}^{PO} = \begin{cases} 2 \hat{n} \times \vec{H}_{inc} & \text{illuminated region} \\ 0 & \text{shadowed region} \end{cases} \quad (4)$$

with the outward pointing normal vector \hat{n} and the incident magnetic near-field \vec{H}_{inc} . Note that this is not the impressed magnetic near-field of the excitation (which is used in the MoM formulation as the known right-hand side), but this is the incident field, comprised of the impressed field plus the magnetic field radiated by the MoM currents.

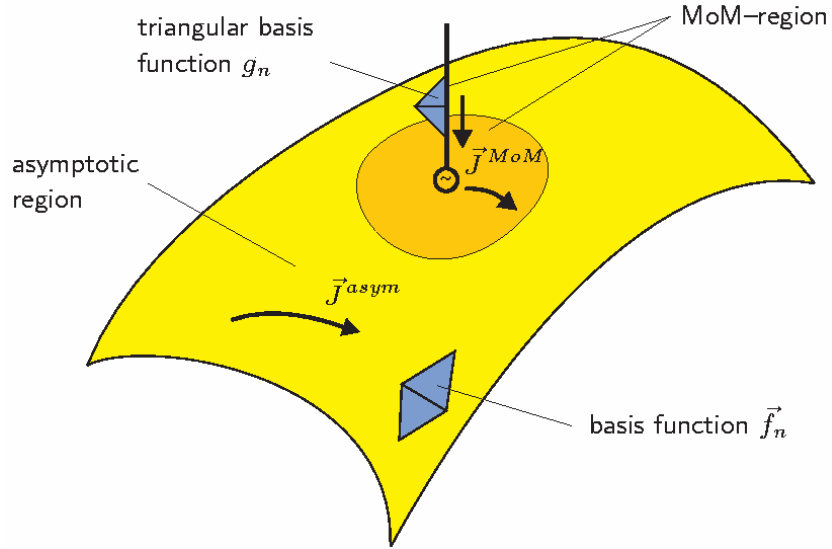


Fig. 6: General idea of splitting the domain into the MoM and an asymptotic region for the current based hybrid method.

More details and also equations for the whole solution procedure of this current based hybrid method can be found in [15, 22].

The PO formulation works reasonably well, but in particular for structures not too big, the accuracy can be improved by either switching to the Physical Theory of Diffraction (PTD) [23, 24], or as we do by adding correction terms to PO (improved PO, IPO) [25, 26] or by switching to Fock currents for curved convex surfaces [27].

As an example, we go back to the aircraft model already considered in Fig. 5. The whole setup is shown in Fig. 7, where this aircraft is standing on the taxiway (150 m parallel to the runway) and

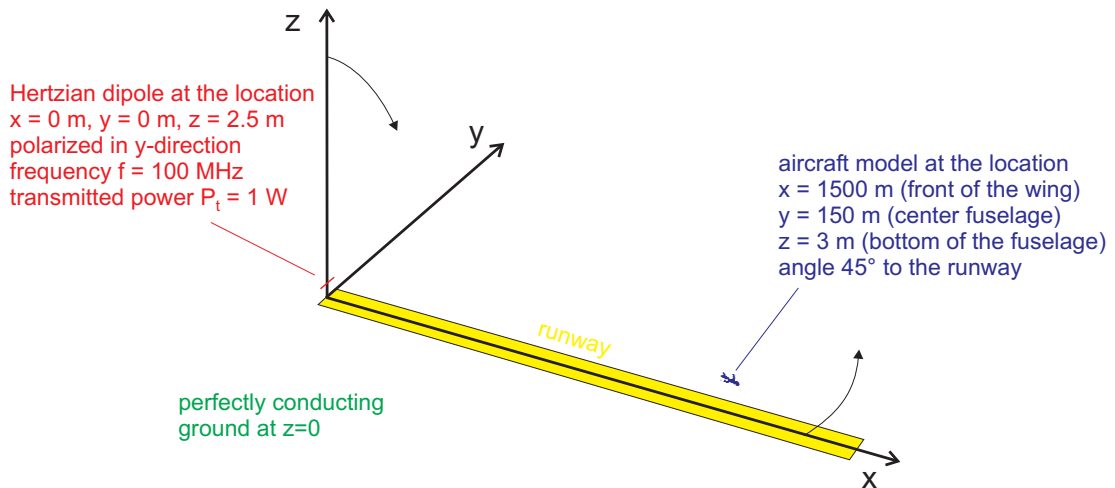


Fig. 7: Runway at an airport with the antenna systems for the instrumental landing system and a parasitic aircraft queuing at the taxiway.

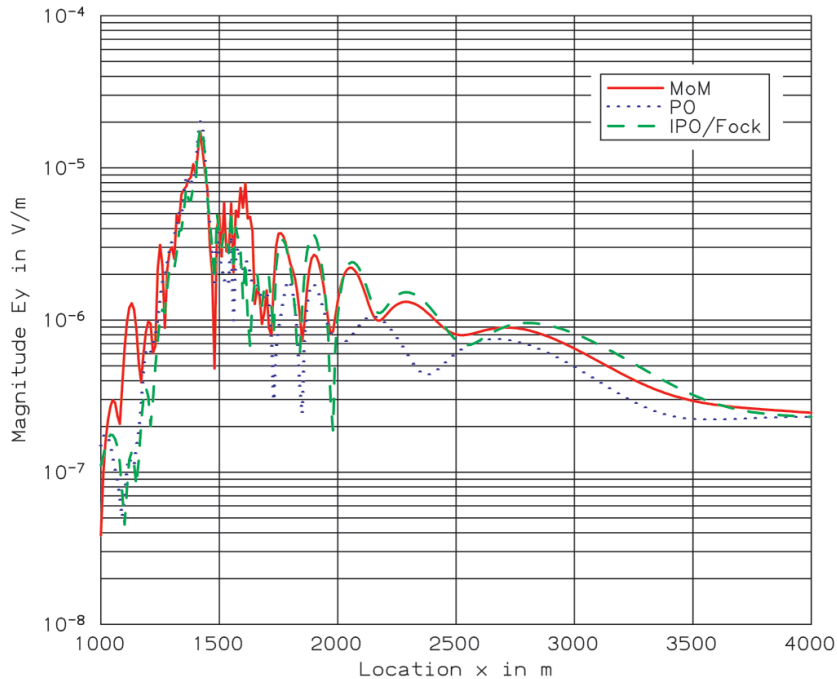


Fig. 8: Disturbance of the landing signal along the runway at an airport due to the presence of an aircraft on the taxiway. Comparison of different numerical techniques.

waiting for take off. This aircraft acts as metallic obstacle which interferes with the instrumental landing system for incoming aircraft.

This disturbance (difference to the signal without the aircraft) is plotted in Fig. 8 along the runway at a height of $z = 3$ m, and the results for the traditional MoM are compared to the asymptotic PO and IPO/Fock solutions. For the practical application, the maximum of these curves is the most important quantity, and this is very similar indeed for the three methods.

As already mentioned, for the traditional MoM the memory requirement is 13.7 GByte. Both the PO and IPO/Fock solutions do need only 10.2 MByte, i.e. a factor 1375 less. Also the run-time of the PO solution is by a factor 560 less than for the MoM. The IPO/Fock solution is a bit more time consuming due to the evaluation of special Fock Airy functions and more sophisticated ray tracing following geodesic lines etc., but it is also a factor of 80 faster than the MoM.

3.3 Ray based hybrid method

The current based hybrid method as presented in the previous section clearly reduces the cost of the MoM from N^2 (memory) and N^3 (run-time) to N for both. This dependency proportional to N is a consequence of discretizing the asymptotic domain, and thus the geometrical data (positions, edge length etc.) for N basis functions have to be stored, and when computing scattered near- or far-fields, one has to loop over the N basis functions and sum the contributions.

For very large problems like a co-site interference study on a ship (see Fig. 9) involving also antennas operating in the GHz frequency range, this dependency on N might still be too large.

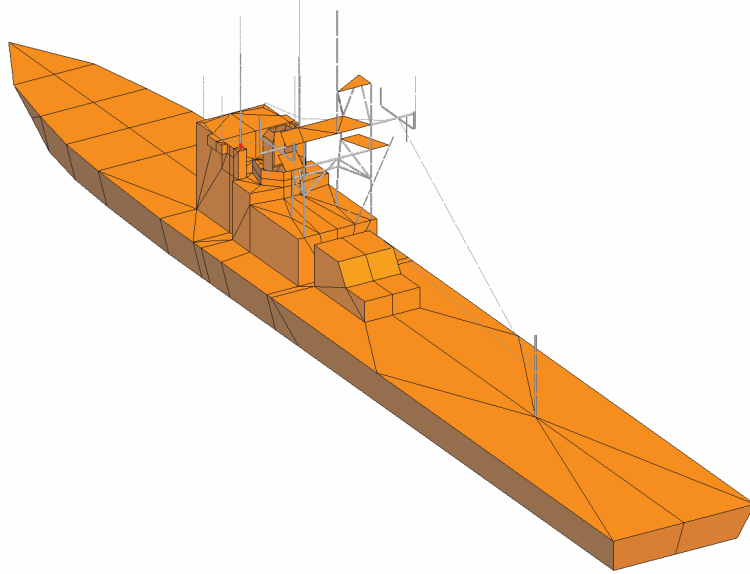


Fig. 9: Antenna coupling study on a ship.

The preferred method in this case is a combination of MoM (for the antennas) with the Uniform Theory of Diffraction (UTD, for the ship body). Then the computational cost with respect to memory and run-time is completely frequency independent. The same resources are required, whether we model antennas at 1 GHz, 10 GHz, or 100 GHz.

Such a combined MoM/UTD hybrid technique has been proposed in a number of early papers, e.g. [28,29]. The formulation regarding our combination of MoM with UTD can be found in [30,31]. There also details are given of how the UTD reflection coefficients have been modified in order to allow MoM sources to be very close (even touching) the UTD region.

3.4 Fast integral equation methods

As mentioned in the introduction, there is no computational technique which can claim to be the best, and which is applicable to all possible scenarios. This is also true for to the current- and ray-based hybrid methods presented in the previous sections. They are extremely useful for a variety of problems, but there are also situations where they cannot be applied, or turn out to be inefficient. We have made several extensions, such as allowing the treatment of dielectric bodies also with PO (see [32]), or including multiple PO reflections, or supporting the treatment of coated surfaces with PO (see [33]). But for instance for convex interior problems, the evaluation of multiple PO reflections is quite time-consuming, and UTD cannot always be used (need for canonical structures with known diffraction coefficients).

Here fast integral equation methods [34–37] can be very useful, they are as general as the MoM regarding the applicability, but have a highly reduced numerical cost. We have focused on a MLFMM (multilevel fast multiple method) implementation in FEKO, where memory scales with $N \log N$, and the CPU-time with $N \log^2 N$.

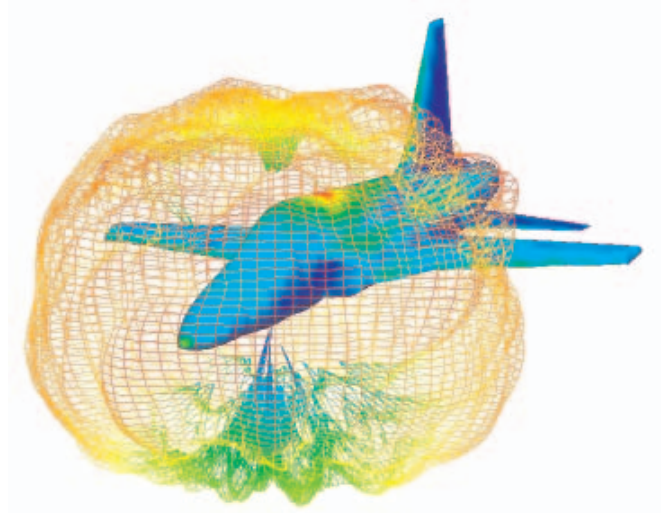
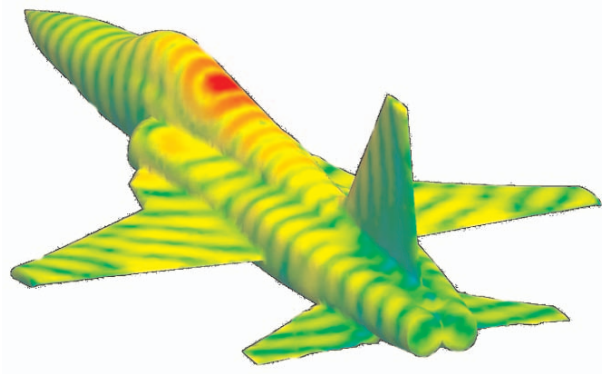


Fig. 10: Surface current density (left) as well as far-field radiation pattern (right) for antenna placement on an aircraft in the 300 MHz UHF frequency band.

In order to show the potential saving as compared to the MoM, two examples shall be considered. The first one is shown in Fig. 10, and deals with antenna placement in the 300 MHz UHF frequency band on an aircraft. The structure consists of 28 634 basis functions, and can still be solved by the traditional MoM, then requiring 12.2 GByte of memory. The MLFMM (here using 6 levels), on the other hand, just requires 437 MByte (this includes everything, also the relatively large memory of 224 MByte for the ILUT preconditioner).

We have also solved a somewhat larger problem, the bistatic RCS computation of a perfectly conducting sphere with a diameter of 10.264λ , resulting in $N = 100005$ unknowns. The advantage of this geometry is that an exact Mie series solution exists to compare the result to (the problem is too big to be solved with the traditional MoM as reference, memory requirement 149 GByte). Both this exact and the MLFMM results are plotted in Fig. 11. A good agreement can be observed, also for the larger angles ϑ (the plane wave is incident from $\vartheta = 180^\circ$, thus $\vartheta = 180^\circ$ corresponds to the backscattering).

The run-time for this specific example is 14 hours on an Intel Pentium 4 PC with 1.8 GHz clock rate. It should be mentioned that this is for the EFIE, although for this specific sphere example the MFIE or CFIE would result in much faster solutions. But see the general discussion in Section 2 of why we prefer to use the EFIE.

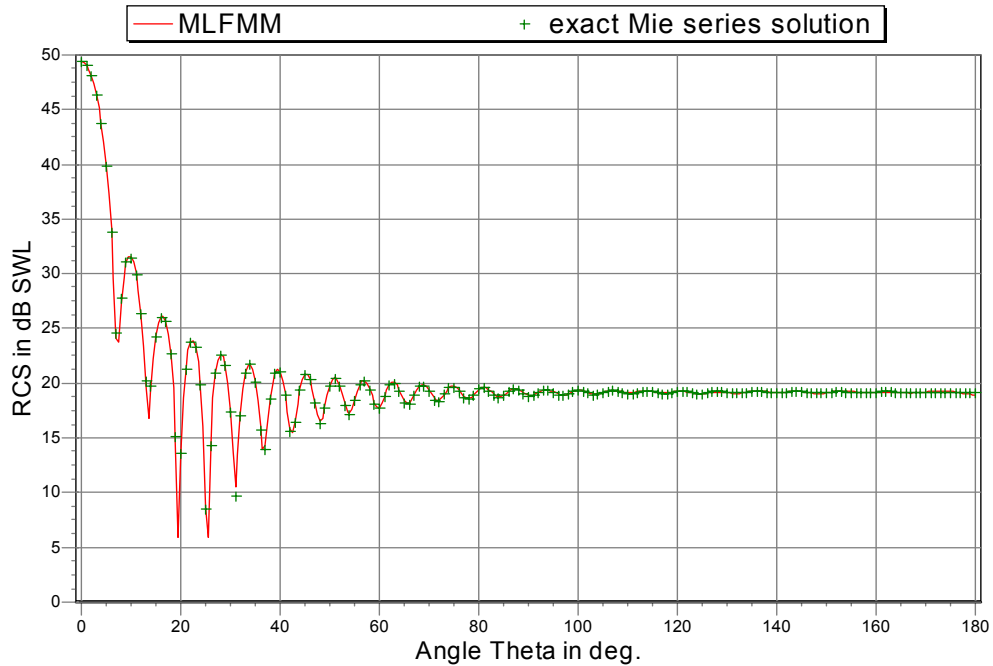


Fig. 11: Bistatic RCS computation for a perfectly conducting sphere of diameter 10.264λ with the MLFMM and comparison to the exact Mie series solution.

4 Conclusions

We have presented an overview on some advanced modeling techniques based on the method of moments, which allow the solution of electromagnetic radiation and scattering problems for a wide frequency range. For the higher frequencies, current- or ray-based hybrid techniques have been proposed (depending on the specific problem at hand), in addition to the popular fast integral equation techniques.

References

- [1] EM Software & Systems - S.A. (Pty) Ltd, Stellenbosch, South Africa, *FEKO — Field Computations Involving Bodies of Arbitrary Shape*, 2003. <http://www.feko.info>.
- [2] T. Itoh, *Numerical Techniques for Microwave and Millimeter-Wave Passive Structures*. John Wiley and Sons, 1989.
- [3] M. N. O. Sadiku, *Numerical Techniques in Electromagnetics*. Boca Raton: CRC Press, 1992.
- [4] A. F. Peterson, S. L. Ray, and R. Mittra, *Computational Methods for Electromagnetics*. IEEE Press, New York, 1998.
- [5] R. F. Harrington, *Field Computation by Moment Methods*. New York: Macmillan Company, 1968.
- [6] S. M. Rao, D. R. Wilton, and A. W. Glisson, “Electromagnetic scattering by surfaces of arbitrary shape,” *IEEE Transactions on Antennas and Propagation*, vol. 30, pp. 409–418, May 1982.

- [7] N. C. Albertsen, J. E. Hansen, and N. E. Jensen, "Computation of radiation from wire antennas on conducting bodies," *IEEE Transactions on Antennas and Propagation*, vol. 22, pp. 200–206, Mar. 1974.
- [8] E. H. Newman and D. M. Pozar, "Electromagnetic modeling of composite wire and surface geometries," *IEEE Transactions on Antennas and Propagation*, vol. 26, pp. 784–789, Nov. 1978.
- [9] A. W. C. Chu, S. A. Long, and D. R. Wilton, "The radiation pattern of a monopole antenna attached to a conducting box," *IEEE Transactions on Antennas and Propagation*, vol. 38, pp. 1907–1912, Dec. 1990.
- [10] S. M. Rao, *Electromagnetic Scattering and Radiation of Arbitrarily-Shaped Surfaces by Triangular Patch Modeling*. PhD thesis, University of Mississippi, 1980.
- [11] D. Zheng and K. A. Michalski, "Analysis of coaxially fed microstrip antennas of arbitrary shape with thick substrates," *Journal of Electromagnetic Waves and Applications*, vol. 5, no. 12, pp. 1303–1327, 1991.
- [12] D. R. Wilton and S. U. Hwu, "JUNCTION: a computer code for the computation of radiation and scattering by arbitrary conducting wire/surface configurations," in *Proceedings of the 5th Annual Review of Progress in Applied Computational Electromagnetics, Monterey*, pp. 43–51, ACES, Mar. 1989.
- [13] A. J. Poggio and E. K. Miller, "Integral equation solutions of three-dimensional scattering problems," in *Computer Techniques for Electromagnetics* (R. Mittra, ed.), ch. 4, pp. 159–264, Oxford: Pergamon Press, 1973.
- [14] N. Morita, N. Kumagai, and J. R. Mautz, *Integral Equation Methods for Electromagnetics*. Boston: Artech House, 1990.
- [15] U. Jakobus and F. M. Landstorfer, "Improved PO–MM hybrid formulation for scattering from three-dimensional perfectly conducting bodies of arbitrary shape," *IEEE Transactions on Antennas and Propagation*, vol. 43, pp. 162–169, Feb. 1995.
- [16] C. W. Trueman and S. R. Mishra, "A WWW–based data base for code validation," in *ACES 12th Annual Review of Progress in Applied Computational Electromagnetics*, vol. II, pp. 1092–1099, Mar. 1996.
- [17] C. L. Larose, C. W. Trueman, and S. R. Mishra, "Measured RCS polar contour maps for code validation," *Applied Computational Electromagnetics Society Journal*, vol. 11, pp. 25–43, Nov. 1996.
- [18] U. Jakobus, "Comparison of different techniques for the treatment of lossy dielectric/magnetic bodies within the method of moments formulation," *AEÜ International Journal of Electronics and Communications*, vol. 54, no. 3, pp. 163–173, 2000.
- [19] B. M. Kolundžija, "Electromagnetic modeling of composite metallic and dielectric structures," *IEEE Transactions on Microwave Theory and Techniques*, vol. 47, pp. 1021–1032, July 1999.
- [20] H.-O. Ruoß, U. Jakobus, and F. M. Landstorfer, "Efficient EM analysis of hand-held mobile telephones close to human head using modified method of moments," *Electronics Letters*, vol. 31, pp. 947–948, June 1995.
- [21] J. J. van Tonder and U. Jakobus, "Full-wave analysis of arbitrarily shaped geometries in multilayered media," in *14th International Zurich Symposium on Electromagnetic Compatibility*, pp. 459–464, Feb. 2001.
- [22] U. Jakobus and F. M. Landstorfer, "Current-based hybrid moment method analysis of electromagnetic radiation and scattering problems," *Applied Computational Electromagnetics Society Journal*, vol. 10, pp. 38–46, Nov. 1995. Special Issue on Advances in the Application of the Method of Moments to Electromagnetic Radiation and Scattering Problems.

- [23] P. Y. Ufimtsev, Метод краевых волн в физической теории дифракции (*The Method of Edge Waves in the Physical Theory of Diffraction*). Москва: Советское Радио Пресс, 1962.
- [24] P. Y. Ufimtsev, “Elementary edge waves and the physical theory of diffraction,” *Electromagnetics*, vol. 11, pp. 125–160, 1991.
- [25] U. Jakobus and F. M. Landstorfer, “Improved physical optics approximation for flat polygonal scatterers,” in *11th International Zurich Symposium on Electromagnetic Compatibility*, pp. 355–360, Mar. 1995.
- [26] U. Jakobus and F. M. Landstorfer, “Improvement of the PO–MoM hybrid method by accounting for effects of perfectly conducting wedges,” *IEEE Transactions on Antennas and Propagation*, vol. 43, pp. 1123–1129, Oct. 1995.
- [27] U. Jakobus and F. M. Landstorfer, “Hybrid MM–PO–Fock analysis of monopole antennas mounted on curved convex bodies,” in *Conference Proceedings of the 12th Annual Review of Progress in Applied Computational Electromagnetics*, (Monterey), pp. 101–108, Applied Computational Electromagnetics Society, Mar. 1996.
- [28] E. P. Ekelman and G. A. Thiele, “A hybrid technique for combining the moment method treatment of wire antennas with the GTD for curved surfaces,” *IEEE Transactions on Antennas and Propagation*, vol. 28, pp. 831–839, Nov. 1980.
- [29] G. A. Thiele and T. H. Newhouse, “A hybrid technique for combining moment methods with the geometrical theory of diffraction,” *IEEE Transactions on Antennas and Propagation*, vol. 23, pp. 62–69, Jan. 1975.
- [30] U. Jakobus and F. M. Landstorfer, “A combination of current– and ray–based techniques for the efficient analysis of electrically large scattering problems,” in *Conference Proceedings of the 13th Annual Review of Progress in Applied Computational Electromagnetics*, (Monterey), pp. 748–755, Applied Computational Electromagnetics Society, Mar. 1997.
- [31] I. P. Theron, D. B. Davidson, and U. Jakobus, “Extensions to the hybrid method of moments/uniform GTD formulation for sources located close to a smooth convex surface,” *IEEE Transactions on Antennas and Propagation*, vol. 48, pp. 940–945, June 2000.
- [32] U. Jakobus, “Extension of the MoM/PO hybrid technique to homogeneous dielectric bodies,” in *Conference Proceedings of the 14th Annual Review of Progress in Applied Computational Electromagnetics*, vol. II, (Monterey), pp. 920–927, Applied Computational Electromagnetics Society, Mar. 1998.
- [33] U. Jakobus and I. P. Theron, “Treatment of coated metallic surfaces with physical optics for the solution of high–frequency EMC problems,” in *15th International Zurich Symposium on Electromagnetic Compatibility*, pp. 257–261, Feb. 2003.
- [34] E. Bleszynski, M. Bleszynski, and T. Jaroszewicz, “AIM: Adaptive integral method for solving large–scale electromagnetic scattering and radiation problems,” *Radio Science*, vol. 31, pp. 1225–1251, Sept. 1996.
- [35] W. C. Chew, J.-M. Jin, C.-C. Lu, E. Michielssen, and J. M. Song, “Fast solution methods in electromagnetics,” *IEEE Transactions on Antennas and Propagation*, vol. 45, pp. 533–543, Mar. 1997.
- [36] C.-C. Lu and W. C. Chew, “A multilevel algorithm for solving a boundary integral equation of wave scattering,” *Microwave and Optical Technology Letters*, vol. 7, pp. 466–470, July 1994.
- [37] R. Coifman, V. Rokhlin, and S. Wandzura, “The fast multipole method for the wave equation: A pedestrian prescription,” *IEEE Antennas and Propagation Magazine*, vol. 35, pp. 7–12, June 1993.

ANALYSIS OF THE TRANSITION BETWEEN TWO COPLANAR WAVEGUIDE TRANSMISSION LINES

Abdelnasser A. Eldek, Atef Z. Elsherbeni and Charles E. Smith

Center of Applied Electromagnetic Systems Research (CAESR), Department of Electrical Engineering The University of Mississippi University, MS 38677

ABSTRACT: *Different approaches for the transition between two coplanar waveguides of different characteristic impedances have been investigated to improve the efficiency of both feeding network and the antenna element of an antenna system operating in the X-band. Return loss, effect of feed line shaping and parametric study are presented with each approach. The outcomes of this study leads to efficient transition between the antenna element and its feeding network.*

Key words: Transition, Coplanar Waveguide, X-Band

1. INTRODUCTION

Transitions between different configurations of planar transmission line become very important in many recent applications. As a result, researchers have tried to introduce the proper transitions in terms of low reflections and insertion loss. The transitions and mode conversion at the transitions from coplanar waveguide (CPW) to 50 Ω grounded CPW (GCPW), and 50 Ω microstrip line are recently studied in [1] and [2] respectively. CPW to CPW transition is introduced through GCPW and microstrip line in [3]. Another study for vertical transition between two CPW is introduced in [4]. However, all these research applications are addressing the transition between two 50 Ω feed lines. In this paper, the transitions between a 50 Ω and non-50 Ω CPW are introduced.

In the design process of antennas, designer usually use the feed line parameters as tuning parameters for controlling both reflection level and bandwidth (BW). The coplanar patch antennas presented in [5], named designs 1 through 4, operating in wireless communication frequency bands, have coplanar waveguides (CPW) of characteristic impedances equal to 70.4, 86.4, 96.4 and 117.17 Ω , respectively, and the BW of these designs reach up to 22.2%. Similarly, The antennas presented in [6], operating in the X-band, do not have 50 Ω feeding line, however, they are designed to cover the 8-12 GHz band. These antennas are usually fed by existing 50 Ω lines, therefore, efficient transition between a non-50 Ω CPW and a 50 Ω CPW is required to maintain the antenna characteristics.

The starting point of this study began with a bow-tie slot antenna which covers the entire X-band from 8 to 12 GHz, with 40% BW. The antenna is simulated using the commercial computer software package, Momentum of Agilent Technologies, Advanced Design System (ADS), which is based on the method of moment (MoM) technique for layered media. Momentum solves mixed potential integral equations (MPIE) using full wave Green's

functions [7]. The antenna is also simulated using the finite difference time domain (FDTD) technique, and good agreement between both results is obtained. The antenna is fed by a CPW of $(W, G) = (3, 0.25)$ mm, where W is the feed line width and G is the gap or slot width. The substrate is RT/duriod 5880 of height equals 1.57 mm and dielectric constant equals 2.2. The characteristic impedance of the CPW of these dimensions is found to be 60.87 Ω , using LineCalc software of ADS. Since the antenna is required to be fed by a 50 Ω line, a transition between the 60.87 Ω and 50 Ω CPWs is required to be studied for minimum reflections and maximum bandwidth throughout the X-band. Three approaches have been investigated for this application, namely the direct connection to the antenna without any transitions and the connection of the antenna feed line to a wider CPW through both an angled and perpendicular slot line. All dimensions shown in the figures are in mm.

2. RESULTS AND ANALYSIS

First Approach

The first approach is to connect the feed line of the antenna directly to a 50 Ω CPW. In this approach, W is kept the same; 3 mm, and G is adjusted for 50 Ω characteristic impedance. Using LineCalc, a CPW of $(W, G) = (3, 0.1044)$ mm, and the same type of substrate is considered. Figure 1 shows the combination of the antenna and the 50 Ω CPW feed line of length L . The return loss of the combination while varying L is shown in Fig. 2, compared with the return loss of the original antenna. This approach gives excellent results as shown in Fig. 2. The return loss of the feeding CPW is studied separately for different L values, as shown in Fig. 3. The return loss is almost less than 40 dB in the X-band. To examine the effect of deforming the CPW feed lines, often required for the feeding network, a simple configuration is shown in Fig. 4, with different horizontal extension length, L . With different values of L , the BW still covers the entire X-band.

Second Approach

The second approach is to connect the feed line of the antenna to a wider 50 Ω CPW through angled slot line. This combination is shown in Fig. 5, where d is the vertical length between the two CPWs. The 50 Ω CPW has $(W, G) = (11, 0.3)$ mm and the same type of substrate, as determined by LineCalc. The return loss of the combination while varying d is shown in Fig. 6, compared with the return loss of the original antenna. As d equals to multiples of $\lambda_g/2$, the BW is nearly the same as that of the original antenna. When $d = 0$, good return loss is obtained, thus, further investigation for this condition is performed as part of the third approach. The return loss of the CPW feedline together with the angled slot line is studied separately for different d values, as shown in Fig. 7. The return loss is almost less than 16 dB in the X-band range.

Third Approach

The third approach is a special case of the second one, where $d = 0$ and (W, G) equal $(11, 4)$ mm, and the

thickness of the perpendicular slot, t , is tapered for matching between the two CPWs. Figure 8 shows this combination of the antenna, the perpendicular slot of thickness t and a $50\ \Omega$ CPW feed line. When t is decreased from 0.35 to 0.20 mm in 0.05 mm steps, the BW increases as shown in Fig. 9, and becomes almost constant when t is in the range 0.18 to 0.15 mm, then starts to decrease as shown in Fig. 10 for $t = 0.1$ and 0.06 mm. By using non-uniform horizontal slot thickness, where t is larger at the $50\ \Omega$ CPW and smaller at the $60.87\ \Omega$, better results are obtained, as shown in Fig. 11, where t varies from 0.1 to 0.25, 0.3 and 0.35 mm. The return loss of the feeding CPW connected with a horizontal slot is studied separately for $t = 0.15, 0.18$ and 0.2 mm and for a non-uniform t that varies from 0.1 to 0.3 and 0.35 mm. As shown in Fig. 12, the maximum return loss for $t = 0.2$ and 0.18 mm is 22 dB, while Fig. 13 shows that the non-uniform cases give return loss smaller than 25 dB. The effect of the length of the $50\ \Omega$ CPW is also studied as shown in Fig. 14, where the BW remains almost constant. To examine the possibility of an offset or redirection of the CPW feedline, a simple offset to the CPW, as shown in Fig. 15, is studied for different horizontal extension length, L with thickness = 0.3 mm. With different values of L , the BW still covers the entire X-band. By varying the thickness of the horizontal slot from 0.1 to 0.3 as shown in Fig. 16, the return loss showed noticeable improvement throughout the X-band frequency range.

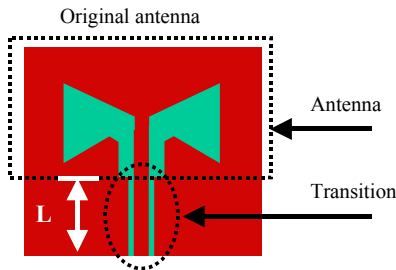


Fig. 1. First type of transition with direction connection.

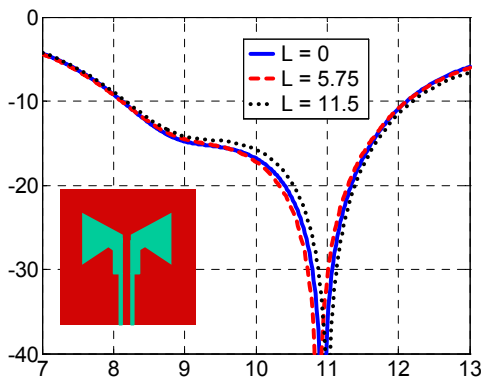


Fig. 2. S11 of the antenna with direct connection to a CPW transition for different L values.

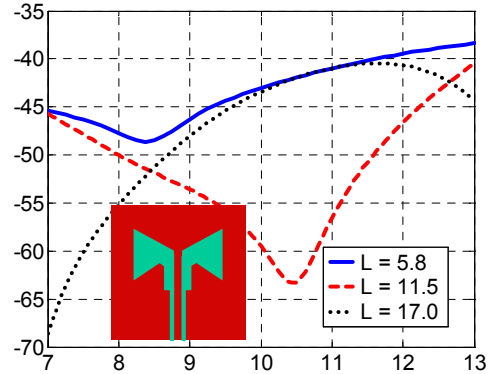


Fig. 3. S11 of the transition with in direct connection.

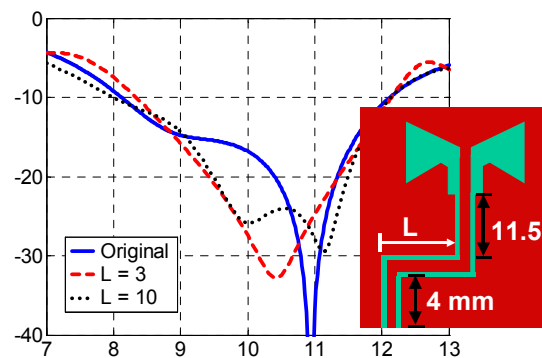


Fig. 4. S11 of the antenna with direct connection to deformed CPW line.

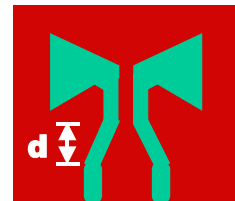


Fig. 5. Antenna connected to the second type of CPW transition.

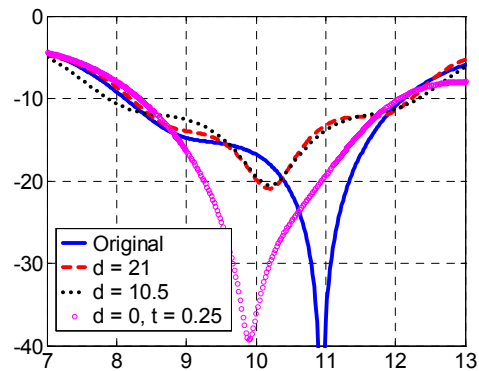


Fig. 6. S11 of the antenna connected to the second type transition with different d values.

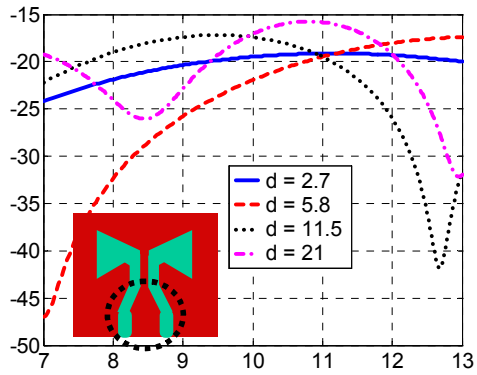


Fig. 7. S11 of the second type transition with the 50 Ω CPW of length 5.8 mm.

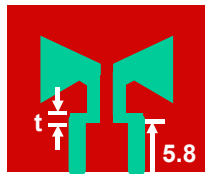


Fig. 8. Antenna connection by the third type approach.

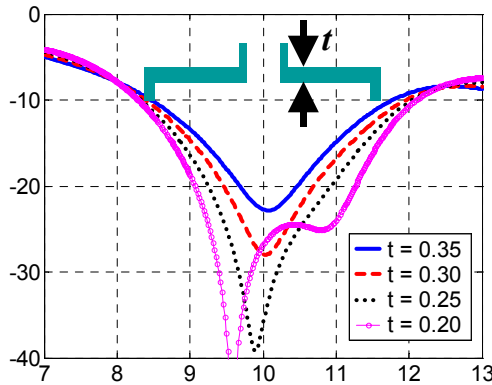


Fig. 9. S11 of the antenna connected to the third type transition with uniform slot thickness changing from 0.35 to 0.2 mm.

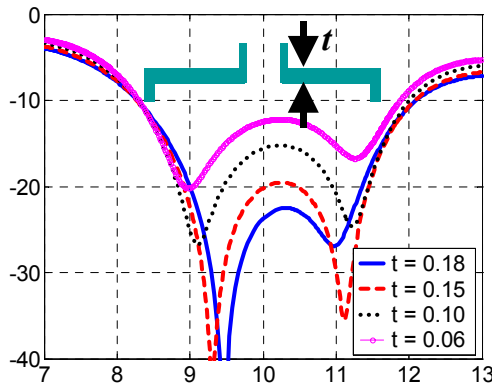


Fig. 10. S11 of the antenna connected to the third type transition with uniform slot thickness changing from 0.18 to 0.06 mm.

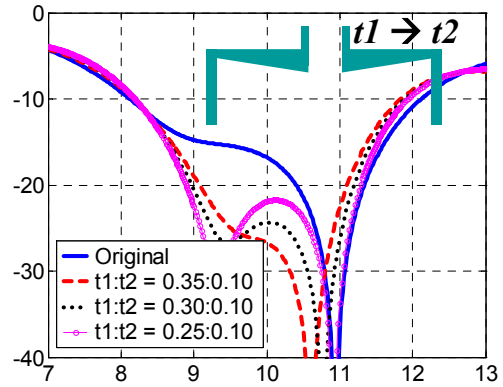


Fig. 11. S11 of the antenna connected to the third type transition with non-uniform slot thickness.

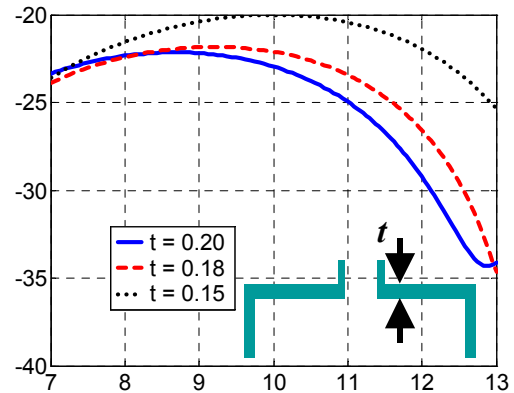


Fig. 12. S11 of the perpendicular slot transition with uniform thickness and the 50 Ω CPW of length 5.8 mm.

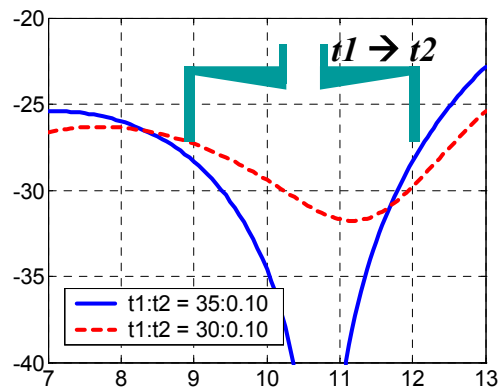


Fig. 13. S11 of the perpendicular slot transition with non-uniform thickness and the 50 Ω CPW of length 5.8 mm.

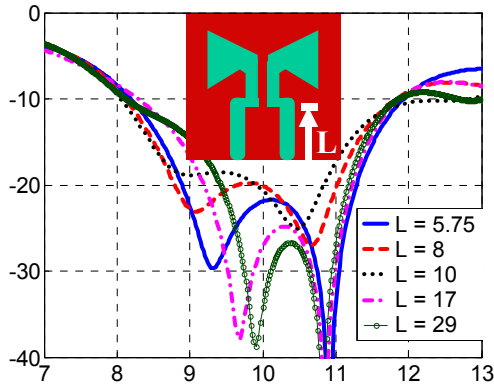


Fig. 14. Effect of changing in L on the return loss of the antenna while connected to the third type transition. The parameter t changes from 0.25 to 0.1 mm.

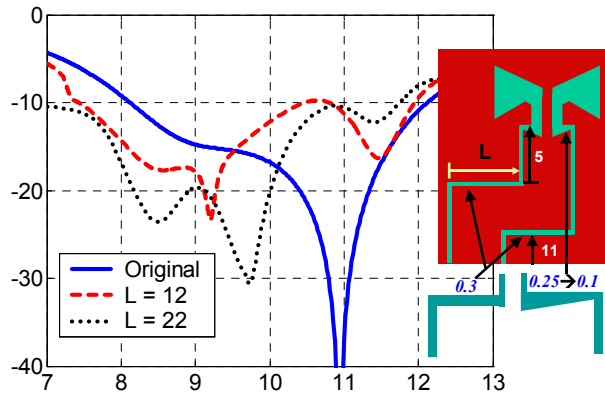


Fig. 15. S_{11} of the antenna connected to the third type transition with deformed line. The lower perpendicular slot has uniform thickness.

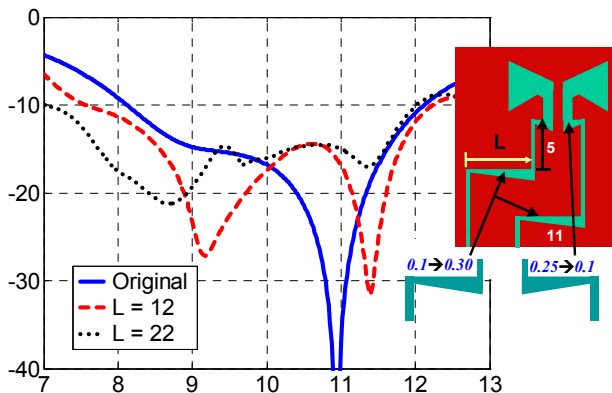


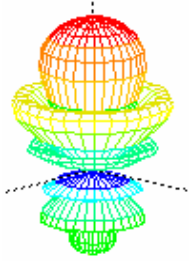
Fig. 16. S_{11} of the antenna connected to the third type transition with deformed line. The lower perpendicular slot has non-uniform thickness.

3. CONCLUSION

Three approaches for the transition between two coplanar waveguides, one of 60.87Ω and the other of 50Ω , have been investigated to reduce the reflection resulting from the transition and to improve the overall efficiency of an antenna system operating in X-band. The direct connection of two CPWs of the same feed line width, yielded excellent performance regardless of the length of the CPW. For unequal feed lines, the connection through angled slot line of length equal to multiples of $\lambda/2$, the bandwidth changes are insignificant. However, for the connection between two unequal feed lines through a horizontally tapered slot line, excellent performance is observed.

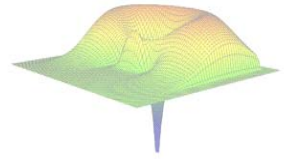
REFERENCES

- [1] Jean-Pierre Raskin, Gildes Gauthier, Linda P. Katehi, and Gabriel M. Rebeiz, "Mode conversion at GCPW-to-microstrip-line transmissions," *IEEE Antenna Trans. Microwave Theory and Techniques*, Vol. 48, No. 1, pp. 158-161, January 2000.
- [2] Amr M. E. Safwat, Kawthar A. Zaki, William Johnson and Chi H. Lee, "Novel transition between different configurations of planar transmission lines," *IEEE Microwave and Wireless Components Letters*, Vol. 12, No. 4, pp. 128-131, April 2002.
- [3] Gildes P. Gauthier, Linda P. Katehi, and Gabriel M. Rebeiz, "W-band finite ground coplanar waveguide (FGCPW) to microstrip line transition," *MTT-S Int. Microwave Symp. Dig.*, pp. 107-109, 1998.
- [4] Jean-Pierre Raskin, Gildes Gauthier, Linda P. Katehi, and Gabriel M. Rebeiz, "W-band single-layer vertical transitions," *IEEE Antenna Trans. Microwave Theory and Techniques*, Vol. 48, No. 1, pp. 161-164, January 2000.
- [5] Abdelnasser A. Eldek, Atef Z. Elsherbeni, Charles E. Smith and Kai-Fong Lee, "Wideband rectangular slot antenna for personal wireless communication systems," *IEEE Antennas and Prop. Magazine*, Vol. 44, No. 5, pp. 146-155, October 2002.
- [6] Abdelnasser A. Eldek, Brad N. Baker, Atef Z. Elsherbeni, Charles E. Smith and Kai-Fong Lee, "Wideband coplanar patch-slot antennas for radar applications," *IEEE International Symb. Antennas and Prop. And URSI National Radio Science meeting*, San Antonio, Texas, Vol. 2, pp. 436-439, July 2002.
- [7] Agilent Technologies, Advance Design Systems 1.5 Momentum, Appendix A, December 2000.



ACES

Applied Computational Electromagnetic Society



ACES Web Site: <http://aces.ee.olemiss.edu>

CALL FOR PAPERS

**The 20th Annual Review of Progress in Applied Computational
Electromagnetics, April 19-23, 2004**
Sheraton Syracuse University Hotel and Conference Center
Syracuse, New York

The 20th Annual Review of Progress in Applied Computational Electromagnetics Symposium will be held for the first time outside Monterey. The location is the Sheraton Syracuse University Hotel and Conference Center in Syracuse, New York, which will accommodate all the technical sessions on the same floor and the lodgings for all the attendees. It is an ideal opportunity to participate in a large gathering of EM analysis enthusiasts. The purpose of the Symposium is to bring developers, analysts, and users together to share information and experience about the practical application of EM analysis using computational methods. The symposium offers technical presentations of all aspects of electromagnetic computational analysis and applications.

Papers may address general issues in applied computational electromagnetics or may focus on specific applications, techniques, codes, or computational issues of potential interest to the applied computational electromagnetics community. All authors of accepted papers will have the option to submit an extended version of their paper or papers for review and publication in special issues of the ACES Journal. Suggested session topics follow, although contributions in other areas of computational electromagnetics are encouraged and will be considered.

Proposed Topics:

Low frequency electromagnetic applications	Time domain methods
Asymptotic and high frequency techniques	Hybrid techniques
Finite element methods	Inverse scattering techniques
Fast and efficient CEM methods	Wave propagation
Wavelet and TLM modeling	MEMS and MMIC
Computational bio-electromagnetics	EMC/EMI
Radar and remote sensing applications	Smart antennas and arrays
Neural network techniques for CEM	Mobile and PCS antennas
Optimization techniques for CEM	RF and microwave devices
Integral or Differential Equations	Phased array antennas
Wideband and multi-frequency antennas	Signal processing antennas

SYMPOSIUM STRUCTURE

The annual ACES Symposium includes: oral-invited sessions, poster sessions, a student paper competition, short courses (*full-day* and *half-day*), an awards banquet, vendor exhibits, and social events. The ACES Symposium will include panel sessions, where invited speakers deliver original essay-like reviews of topics of current interest to the computational electromagnetics community.

PAPER FORMATTING REQUIREMENTS

The recommended paper length, including text, figures, tables and references, is four (4) pages, with eight (8) pages as a maximum. Submitted papers should be formatted for 8.5x11-inch U.S. standard paper, with 1-inch top, bottom and side margins. On the first page, the title should be 1-1/2 inches from top with authors, affiliations, and e-mail addresses beneath the title. **Use single line spacing, with 11- or 12-point size of Times New Roman or Times font. Please do not use Asian fonts. No typed page numbers, headers or footers.** The entire text should be fully justified (flush left and flush right). A model paper can be found in the conference section on ACES web site at: <http://aces.ee.olemiss.edu>. Each paper should be submitted in camera-ready format with good resolution and clearly readable.

PAPER SUBMISSION PROCEDURE

No email, fax or hard-copy paper submission will be accepted. Papers are required, in Adobe Acrobat (version 5 or later) or in Microsoft Word 2000 format and must be submitted through ACES web site using the “Paper Submission” button in the left menu, followed by the selection of the “Conference” option, and then following the on-line submission instructions. Successful submission will be acknowledged automatically by email after completing all uploading procedure as specified on ACES web site.

SUBMISSION DEADLINE AND REGISTRATION REQUIREMENT

Submission deadline is **November 1, 2003**. A signed ACES copyright-transfer form must be mailed to the conference chair immediately following the submission as instructed in the acknowledgment of submission email message. Papers without an executed copyright form will not be considered for review and possible presentation at the conference. Upon the completion of the review process, by the technical program committee, the acceptance notification along with the pre-registration information will be mailed to the corresponding author on or about **December 10, 2003**. Each presenting author is required to complete the paid pre-registration and the execution of any required paper corrections by **February 1, 2004** for final acceptance for presentation and inclusion in the symposium proceedings.

BEST-PAPER PRIZE

A **\$500** prize will be awarded to the authors of the best non-student paper presented (poster or oral) at the 20th Annual Review. Papers will be judged by the ACES prize-paper committee.

BEST STUDENT PAPERS CONTEST

The best three (3) student papers presented at the 20th Annual Review will be announced at the symposium banquet. Student papers submitted for this competition will be judged by three (3) members of the ACES Board of Directors. The first, second, and third winners will be awarded cash prizes of **\$300, \$200, and \$100**, respectively.

For any additional information, including travel and lodging, please contact the conference Chair: **Tapan K. Sarkar** (tk Sarkar@svr.edu, Tel: 315-443-3775, Fax: 315-443-4441), or visit ACES web site at: <http://aces.ee.olemiss.edu>.

Symposium Chair	Symposium Co-Chair	Symposium Administrator	Short Course Chair	Exhibits Chair	Publicity Chair
<i>Tapan K. Sarkar</i>	<i>Atef Elsherbeni</i>	<i>Richard W. Adler</i>	<i>John Shaeffer</i>	<i>Andrew L. Drozd</i>	<i>Omar M. Ramahi</i>
Syracuse University	The University of Mississippi	Naval Postgraduate School	Retired CEM Enthusiast	ANDRO Consulting	University of Maryland

APPLIED COMPUTATIONAL ELECTROMAGNETICS SOCIETY
RICHARD W. ADLER, EXECUTIVE OFFICER
ECE DEPARTMENT, CODE ECAB, 833 DYER ROAD, ROOM 437
NAVAL POSTGRADUATE SCHOOL, MONTEREY, CA 93943-5121,
PHONE: 831-646-1111 FAX: 831-649-0300
EMAIL: RWA@ATTGLOBAL.NET

Please print

LAST NAME	FIRST NAME	MIDDLE INITIAL
COMPANY/ORGANIZATION/UNIVERSITY	DEPARTMENT / MAIL STATION	
MAILING ADDRESS WHERE PUBS MAY BE MAILED		
CITY	PROVINCE/STATE	COUNTRY
		ZIP/POSTAL CODE
TELEPHONE	FAX	AMATEUR RADIO CALL SIGN
		E-MAIL ADDRESS

	NEW MEMBERSHIP RATES (EFFECTIVE JANUARY 2003)			
	BASIC	INTERMEDIATE	EXPANDED	INSTITUTIONAL
	WORLD AREA	Journal & Newsletter Access via Website & Annual (Nov) Searchable CD Rom of Proceedings of March Conference & Searchable CD ROM of year's Journals	BASIC, plus CD ROM of March Journal (Mar) & CD ROM of July Journal (Jul)	BASIC, plus Unbound Paper Copies of Journals (Mar, Jul, Nov)
US, CANADA and MEXICO	\$35. USD	\$55. USD	\$90. USD	\$125. USD
ALL OTHER AREAS	\$35. USD	\$55. USD	\$110. USD	\$125. USD

FULL-TIME STUDENT/RETIRED/UNEMPLOYED: BASIC RATE IS \$20.00 USD FOR ALL COUNTRIES

Non-USA participants: Prices are in U.S. dollars. All currencies must be converted to U.S. dollars payable by banks with U.S. affiliates. (1) Bank Checks must have U.S. address of bank; Checks are payable to "ACES", (2) U.S./International Money Order drawn in U.S. funds, payable in U.S. \$\$, (3) Credit Cards: Visa, MasterCard, Amex and Discover.

CREDIT CARD USERS

PRINT CARD HOLDER NAME: _____

CREDIT CARD HOLDER SIGNATURE: _____

CREDIT CARD HOLDER ADDRESS: _____

ADDRESS, CONT: _____

CREDIT CARD ACCOUNT #: _____

CARD EXP. DATE: _____

2003

ADVERTISING RATES		
	FEE	PRINTED SIZE
Full page	\$200	7.5" × 10.0"
1/2 page	\$100	7.5" × 4.7" or 3.5" × 10.0"
1/4 page	\$50	3.5" × 4.7"
<p>All ads must be camera ready copy.</p> <p>Ad deadlines are same as Newsletter copy deadlines.</p> <p>Place ads with Ray Perez, Newsletter Editor, Martin Marietta Astronautics, MS 58700, PO Box 179, Denver, CO 80201, USA. The editor reserves the right to reject ads.</p>		

DEADLINE FOR THE SUBMISSION OF ARTICLES	
Issue	Copy Deadline
March	February 1
July	June 1
November	October 1

For the **ACES NEWSLETTER**, send copy to Bruce Archambeault in the following formats:

1. A PDF copy. Do NOT page number the document!
2. A MS Word (ver. 97 or higher) copy. If any software other than WORD has been used, contact the Managing Editor, Richard W. Adler **before** submitting a diskette, CD-R or electronic file.